AD-A041 199 STATE UNIV OF NEW YORK AT ALBANY F/G 20/14
SCATTERING OF ELECTROMAGNETIC RADIATION BY APERTURES: XI. THE O--ETC(U)
MAR 77 J P HECKL, L F LIBELO, C L ANDREWS N60921-75-C-0131
UNCLASSIFIED NSWC/WOL-TR-76-74 NL

1 OF 2
AD A041199

NSWC/WOL/TR 76-74

NSWC/WOL/TR 76-74

12

NSWC TECHNICAL REPORT

WHITE OAK LABORATORY

SCATTERING OF ELECTROMAGNETIC RADIATION BY APERTURES: XI. THE OPEN CYLINDRICAL TUBE OF FINITE LENGTH — AXIAL ELECTRIC FIELD, INTERIOR AND EXTERIOR SURFACE CHARGE DENSITY AND EXTERIOR SURFACE CURRENT DISTRIBUTION

1 MARCH 1977

NAVAL SURFACE WEAPONS CENTER
WHITE OAK LABORATORY
SILVER SPRING, MARYLAND 20910

- Approved for public release; distribution unlimited

NAVAL SURFACE WEAPONS CENTER
WHITE OAK, SILVER SPRING, MARYLAND 20910

UNCLASSIFIED

SECURITY CLASSIFICATION OF THIS PAGE (When Data Entered)

REPORT DOCUMENTATION PAGE

READ INSTRUCTIONS BEFORE COMPLETING FORM

1. REPORT NUMBER: NSWC/WOL/TR-76-74
2. GOVT ACCESSION NO.
3. RECIPIENT'S CATALOG NUMBER

4. TITLE (and Subtitle): Scattering of Electromagnetic Radiation by Apertures: XI. The Open Cylindrical Tube of Finite Length - Axial Electric Field, Interior and Exterior Surface Charge Density and Exterior Surface Current Distribution

5. TYPE OF REPORT & PERIOD COVERED: Topical Rept.

6. PERFORMING ORG. REPORT NUMBER

7. AUTHOR(s): J. P. Heckl (NSWC/WOL), L. F. Libelo (NSWC/WOL), C. L. Andrews (SUNYA), D. P. Margolis (SUNYA)

8. CONTRACT OR GRANT NUMBER(s): N60921-75C-0131

9. PERFORMING ORGANIZATION NAME AND ADDRESS
Naval Surface Weapons Center
White Oak Laboratory
White Oak, Silver Spring, Maryland 20910

10. PROGRAM ELEMENT, PROJECT, TASK AREA & WORK UNIT NUMBERS: 61152N; ZR00001; ZR02101; WR0108;

11. CONTROLLING OFFICE NAME AND ADDRESS

12. REPORT DATE: 1 March 1977

13. NUMBER OF PAGES: 98

14. MONITORING AGENCY NAME & ADDRESS (if different from Controlling Office)

15. SECURITY CLASS. (of this report): UNCLASSIFIED

15a. DECLASSIFICATION/DOWNGRADING SCHEDULE

16. DISTRIBUTION STATEMENT (of this Report)

Approved for public release; distribution unlimited.

17. DISTRIBUTION STATEMENT (of the abstract entered in Block 20, if different from Report)

18. SUPPLEMENTARY NOTES

The effort was funded jointly by the Defense Nuclear Agency, NSWC/WOL under the IR program and the State University of New York at Albany with partial support from NSWC/WOL under contract N60921-75-C-0131. Work was performed in collaboration with SUNY at Albany.

19. KEY WORDS (Continue on reverse side if necessary and identify by block number)
Electromagnet Diffraction
Hollow Finite Circular Tube
Axial Electric Field Inside
Surface Charge Density on Inside and Outside Walls
Outside Surface Current Distribution

20. ABSTRACT (Continue on reverse side if necessary and identify by block number)

Using linearly polarized plane electromagnetic radiation we irradiated finite length, conducting, circular cylinders at normal broadside incidence. These tubes were thin walled, open at both ends and empty. Measurements of the radial electric field component at the axis were made and the results are discussed. For tube dimensions comparable to the wavelength of the incident radiation measurements were also made of the internal and external surface charge densities and the exterior surface current distributions. Comparison with available theory is discussed.

DD FORM 1 JAN 73 1473 EDITION OF 1 NOV 65 IS OBSOLETE
S/N 0102-014-6601

UNCLASSIFIED
SECURITY CLASSIFICATION OF THIS PAGE (When Data Entered)

256 850

1 March 1977

NSWC/WOL/TR 76-74

SCATTERING OF ELECTROMAGNETIC RADIATION BY APERTURES: XI. THE OPEN CYLINDRICAL TUBE OF FINITE LENGTH - AXIAL ELECTRIC FIELD, INTERIOR AND EXTERIOR SURFACE CHARGE DENSITY AND EXTERIOR SURFACE CURRENT DISTRIBUTION.

This report contains the results of an investigation into an electromagnetic diffraction problem. The study was performed jointly in the Physics Department of the State University of New York at Albany, New York and at the Naval Surface Weapons Center, White Oak. At the State University of New York the efforts were partially supported by NSWC/WOL under contract N60921-75-C-0131. At NSWC/WOL the effort was supported partly by the Defense Nuclear Agency under Task DNA-R99QAXEB088 and partly by the Independent Research Program (Task Number MAT-03L-000/ZR011-01-01). This document is for information only.

Paul R. Wessel

PAUL R. WESSEL
By direction

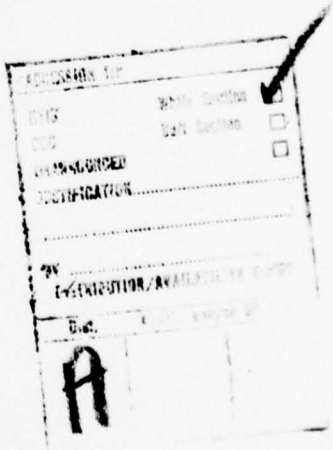

TABLE OF CONTENTS

LIST OF FIGURES

LIST OF FIGURES (Cont.)

I. INTRODUCTION

This paper is a report of empirical results obtained for diffraction of electromagnetic radiation by an empty circular cylindrical tube of finite length. It constitutes another in a sequence of reports[1,2] on our investigations of three dimensional electromagnetic scattering problems possessing intrinsic cylindrical geometry. This sequence of reports is itself only a part of a more extensive series of reports on studies of the scattering and diffraction characteristics of conducting enclosures containing apertures and also the subsequent interaction and coupling of the penetrating radiation to elements contained therein.

In this publication we report on a study of the response of a thin walled, highly conducting, circular cylinder of finite length, wide open at both ends, to linearly polarized monochromatic, plane, electromagnetic radiation at normal broadside incidence. Results obtained for the induced surface current distribution, the surface charge density and the radial component of electric field along the axis are presented. Two separate cases are considered for the incident radiation, namely, E-polarization in which the incident electric field is polarized parallel to the cylinder axis, and H-polarization in which the magnetic field in the incident plane wave is polarized along the cylinder axis. Figure 1 is a simple illustration of the geometry of the diffraction problem for the first case

1. R. L. Kligman, L. F. Libelo, "S.E.R.A. VIII. The Normally Slotted Infinite Cylinder-Theory" NOLTR 74-35 June 1974.
2. L. F. Libelo, C. L. Andrews, "S.E.R.A. IX. Surface Current Distributions Over a Closed Cylindrical Can at Broadside Incidence," NSWC/WOL/TR 75-163 February 1976.

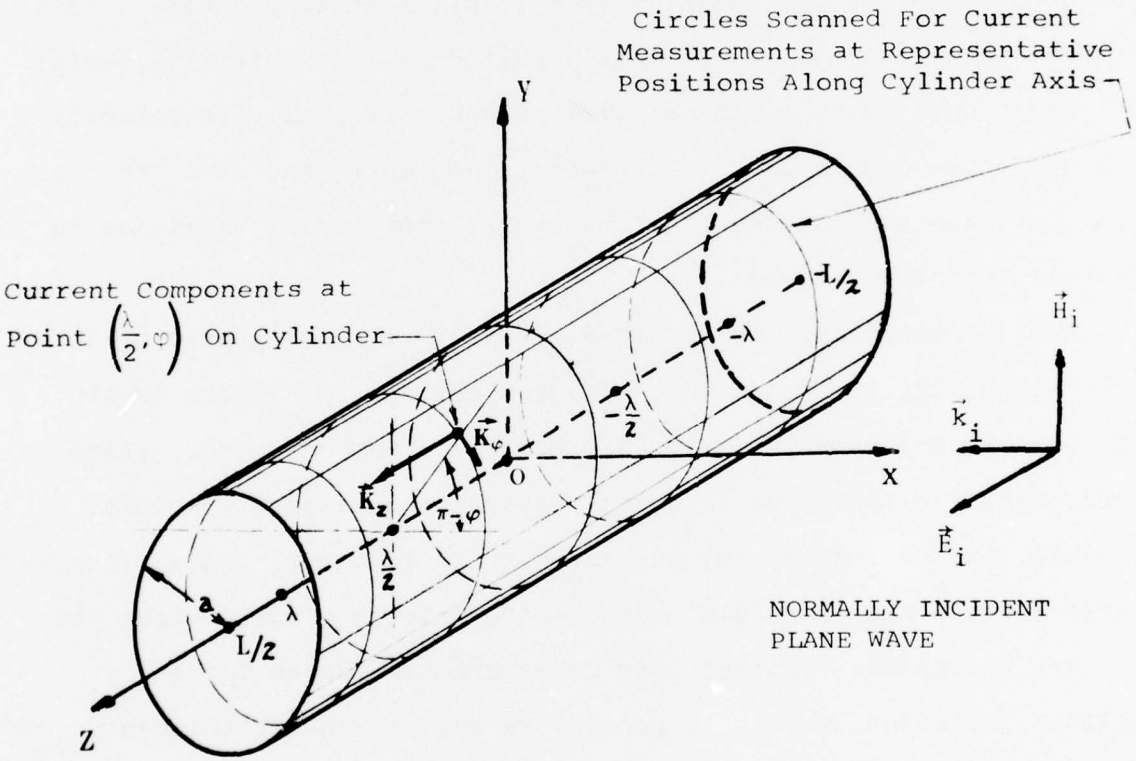

Figure 1. SCATTERING GEOMETRY FOR OPEN ENDED CIRCULAR CYLINDRICAL TUBE OF LENGTH L, RADIUS a.

i.e. E-polarization. For reasons of economy in time and labor the study was focused on each of two representative finite metallic circular cylindrical tubes; the first was 6.125 inches (15.56cm) in diameter and 12 inches (30.48cm) long, and the second cylinder was 7 inches (17.78cm) in diameter and 7 inches in length. Using E-polarized incident radiation at 12.8cm in wavelength measurements were made of the angular and longitudinal components of the surface current along the length and around the circumference of the first cylinder. For the given cylinder dimensions and the incident wavelength the parameters that characterize this problem are the circumference to wavelength ratio $\gamma=2\pi a/\lambda=3.82$ and the ratio of the cylinder length to wavelength which we denote by $2h\equiv L/\lambda=2.38$. Neither parameter can without overstretching the imagination be considered to be a priori asymptotic in value. In addition to the surface current distribution we also measured the surface charge density distribution both over the outer and the inner surfaces. These surface charge densities are given essentially by the normal or radial component of electric field at the surface. Unfortunately the measurements of surface charge density were only obtained for H-polarized incident radiation. Nevertheless the results are still quite useful and informative. The second cylinder was also irradiated at normal broadside incidence with 23.2cm radiation. For this cylinder the two basic parameters are $\gamma=2.40$, for the circumference to wavelength ratio, and $2h=0.766$ for the length to wavelength ratio. Although the second cylinder is in fact shorter than a wavelength

we still are not asymptotic by any means. Measurements of the two surface current components were made over the surface using E-polarized and also H-polarized incident radiation for the shorter cylindrical tube. The surface charge density distribution on the inner and outer surfaces were also measured on this cylinder again only for H-polarized incident radiation. For this second cylinder we also measured the radial component of the electric field along the axis of the tube. This was done for both polarizations of the normally incident radiation. The results, as we shall see below, point out rather interesting behaviour of this field at the tube ends.

Several poignant aspects of this study should be pointed out at the start. These shall be re-emphasized below from time to time where pertinent as the description of the investigation develops. First of all it should be noted that we are working in the difficult regime where the wavelength is comparable to both the length and circumference of the target cylinder. In this range of the parameters γ and $2h$, i.e. beyond the Rayleigh limit and well short of the geometrical optics region, very little is known of the details of the scattering and diffraction characteristics of the circular cylindrical conducting tube of finite length. This is especially true for the case of broadside incidence on the finite metallic cylinder. This range of size to wavelength ratio is commonly referred to as the resonance region. In this region it has been fairly common practice to use the exact solution for the infinite circular conducting

cylinder to approximate to the scattering characteristics for a finite cylinder in particular to the surface currents and charge distributions on the outside surface and also of course the near fields. The exact solution of the problem of scattering by an infinite, perfectly conducting circular cylinder is a well known conventional text-book case and as such is available in many references. We cite only a representative few such references here[3-7]. The same situation obtains for the interior problem.

It is helpful to put this study in a more proper perspective by reviewing the past attempts to investigate this diffraction problem. For this purpose we obviously can only resort to the published papers related to the finite open ended tube. In a preceding publication[8] we presented an extensive literature review of the finite cylinder. In this review we particularly made a point of omitting any reference to the short, fat, empty open ended circular tube. Since these works are of pointed significance here we shall therefore reference them in this paper. Thus, for example, the very thin, open ended, hollow tube references can be found in the previous report.[8]

3. J. Van Bladel, "Electromagnetic Fields" p. 376-382 McGraw-Hill Book Co., New York, N. Y. 1964.
4. J. J. Bowman, T.B.A. Senior and P.L.E. Uslenghi, eds. "Electromagnetic and Acoustic Scattering by Simple Shapes" pp. 92-93, North Holland Co., Amsterdam, the Netherlands 1969.
5. R.W.P. King and T.T. Wu, "Scattering and Diffraction of Waves," p. 38, Harvard Univ. Press, Cambridge, Mass. 1959.
6. W. Panofsky and M. Phillips, "Classical Electricity and Magnetism" p. 199-301 Addison-Wesley Publishing Co., Reading, Mass. 1956.
7. J. R. Wait, "Electromagnetic Radiation from Cylindrical Structures," p. 142, Pergamon Press, New York 1959.
8. L. F. Libelo, C. L. Andrews, "S.E.R.A. IX. Surface Current Distribution over a Closed Cylindrical Can at Broadside Incidence" NSWC/WOL/TR 75-163, February 1976.

For the case of the conducting, circular, empty cylinder of finite length and finite diameter no satisfactory exact analytic general solution has as yet appeared in the literature. Furthermore very little in the way of empirical results have been presented in the open literature. The corresponding problem of the fat open ended finite length cylindrical antenna has been subjected to some study. Although this is not the diffraction problem it is still informative to see the extent to which progress has been made in solving that related problem. T. T. Wu[9] has given an excellent review of the investigative efforts related to this problem. In his review he discusses a fundamental difficulty inherent in the thin walled, circular, open tube of finite length which seriously impedes attempts to analytically solve for the surface currents. Needless to say this problem is also present in the diffraction problem. The major analytic effort in T. T. Wu's presentation deals with very long wavelengths or else thin long tubes. Chang[10,11] in his study of the electrically thick monopole uniformly driven around the circumference, Seshadri and Wu,[12] and Wu and King[13]

---

9. T. T. Wu, "Introduction to Linear Antennas," Chapt. 8 of "Antenna Theory," Part 1 by R. E. Collin and F. J. Zucker, McGraw-Hill Book Company, New York, 1969.
10. D. C. Chang, "On the Electrically Thick Monopole Part I - Theoretical Solution," IEEE Trans. Ant. and Prop. AP-16, 58 (1968).
11. D. C. Chang, "On the Electrically Thick Cylindrical Antenna," Tech. Rept. 509 Cruft Laboratory, Harvard Univ., Cambridge, Mass. 1966.
12. S. R. Seshadri, T. T. Wu, "An Integral Equation for the Current In an Asymmetrically Driven Antenna," Proc. IEEE 55, 1097 (1967).
13. T. T. Wu, R.W.P. King, "The Thick Tubular Transmitting Antenna," Radio Sci., 2, 1088 (1967).

further considered the thick tubular antenna. They found additional constraining difficulties due to the geometry of the problem that seriously inhibit attempts at analytic solution for the finite cylinder. Essentially starting from the analysis presented by T. T. Wu, Kao[14] developed a formal solution for the scattering of electromagnetic radiation by a finite, hollow metallic, thin walled circular cylindrical tube. To achieve this he handled the analytic difficulty in the current problem mentioned above by introducing two parameters that forced the longitudinal current to vanish at the tube ends. He further developed a computer program to numerically solve the problem and published a number of results he obtained.[15-17] To solve the problem numerically he adopted the numerical method of Young.[18-19] To help verify the numerical predictions he performed a series of measurements for the related cylinders and included the

14. C. C. Kao, "Three Dimensional Electromagnetic Scattering From a Circular Tube of Finite Length," Jour. Appl. Phys. 40, 4732 (1969).
15. C. C. Kao, "Electromagnetic Scattering From a Finite Tubular Cylinder: Numerical Solutions and Data I. Development of Theory," AFCRL-69-0535(I) Cruft Laboratory, Harvard Univ., Cambridge, Mass. 1969.
16. C. C. Kao, "Electromagnetic Scattering From a Finite Tubular Cylinder: Numerical Solutions and Data II. Numerical Results," AFCRL-69-0535(II) Cruft Laboratory, Harvard Univ., Cambridge, Mass. 1969.
17. C. C. Kao, "Electromagnetic Scattering From a Finite Tubular Cylinder: Numerical Solutions," Radio Sci. 5, 617 (1970).
18. A. Young, "Approximate Product Integration," Proc. Roy. Soc. A-224, 552 (1954).
19. A. Young, "The Application of Approximate Product-Integration to the Numerical Solution of Integral Equations," Proc. Roy. Soc. A-224, 561 (1954).

empirical results along with the numerical results.[20] We have adapted Kao's program to our computer and have used it to calculate the surface current component distributions for the metal tubes we have subjected to measurement. We show below the results of the comparison. Briefly, we find that the Kao solution appears to be too severely limited in accuracy for any extensive range of parameters. We shall go into further detail below when we present the comparisons. It would appear that there is still no reliable analytic solution to the diffraction problem.

We next present the experimental procedure used to obtain the measurements. Following this we present the empirical results obtained by that method. Next we discuss the results and compare them with existing approximate solutions. Following this we sum up the present situation.

20. C. C. Kao, "Measurements of Surface Currents On a Finite Circular Tube Illuminated by An Electromagnetic Wave," IEEE Trans. on Ant. and Prop. AP-18, 569 (1970).

II. EXPERIMENTAL METHOD

All measurements related to the hollow circular cylindrical tube were made within a tapered anechoic chamber. The advantages of such a chamber configuration have been adequately discussed elsewhere[21] and hence all discussion shall be omitted from this report. The useful range of wavelength for the specific chamber in which the measurement program was carried out is from 1 to 100cm. The length of the chamber is 36 feet (11 meters) and the wide end is about 8 ft (2.4 meters) on a side. At the wide end of the tapered anechoic chamber is a working volume consisting of a cube approximately 30cm on edge. In this working volume called the "quiet zone," QZ, the fields are very nearly uniform plane waves in the absence of a target. At the narrow end short sections of the chamber are demountable to facilitate the placement of microwave horns that serve as the source of the electromagnetic radiation. Figure 2 is a simple schematic illustration of the tapered chamber. It displays in a cutaway top view the "quiet zone" and the position of the absorber covered access door.

To measure the surface current density amplitude we measured the corresponding surface magnetic field amplitude using detectors fabricated from commercially available point-contact silicon crystal diodes of the type 1N82AG. The actual magnetic field probe, shown

---

21. R. O. Dell, C. R. Carpenter and C. L. Andrews, "Optical Design of Anechoic Chambers," Jour. Opt. Soc. Amer., 902, 62 (1972).

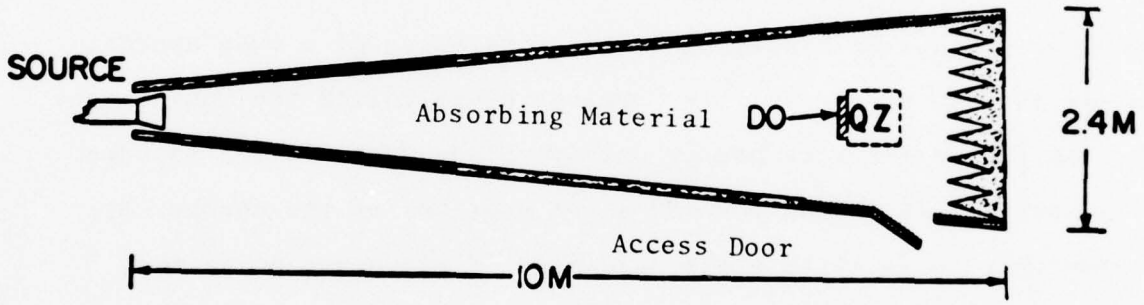

Figure 2. Tapered Anechoic Chamber Utilized In Measurements. Diffracting Object - DO, Quiet Zone - QZ and Radiation Source are Illustrated.

in figure 3, is basically the point-contact diode with attached arms bent so as to form a square loop together with two 10 mil brass plates separated by a 2 mil sheet of mica. In the magnetic field sensor the crystal diode is maintained parallel to the brass plates. The amplitude of a component of surface current at a surface point is found by measuring the square of the amplitude of the tangential component of magnetic field, at that point, that is aligned normal to the current component. Further detailed discussion of such probes is available elsewhere.[22] During the actual measurement of a current the magnetic field detector is fastened to the diffracting finite cylinder itself. Rotating the cylinder with the probe attached to it then permits us to obtain a scan of the surface current over the azimuthal range of position variable. Repeating this scanning of the current by relocating the magnetic field probe produces a mapping of the surface current amplitude over the entire finite circular cylinder. Both the longitudinal and the azimuthal surface current amplitude maps were obtained in this manner (these are essentially the azimuthal and longitudinal magnetic field maps, respectively, very close to the conducting surface). In these measurements the signal is transmitted from the probe via a twisted pair of high impedance 3 mil diameter EVANOHM leads to the recording system.

---

22. C. L. Andrews, A. Golab, "Probe Antennas for Microwave Measurements," Amer. Jour. Phys. 121, 39 (1971).

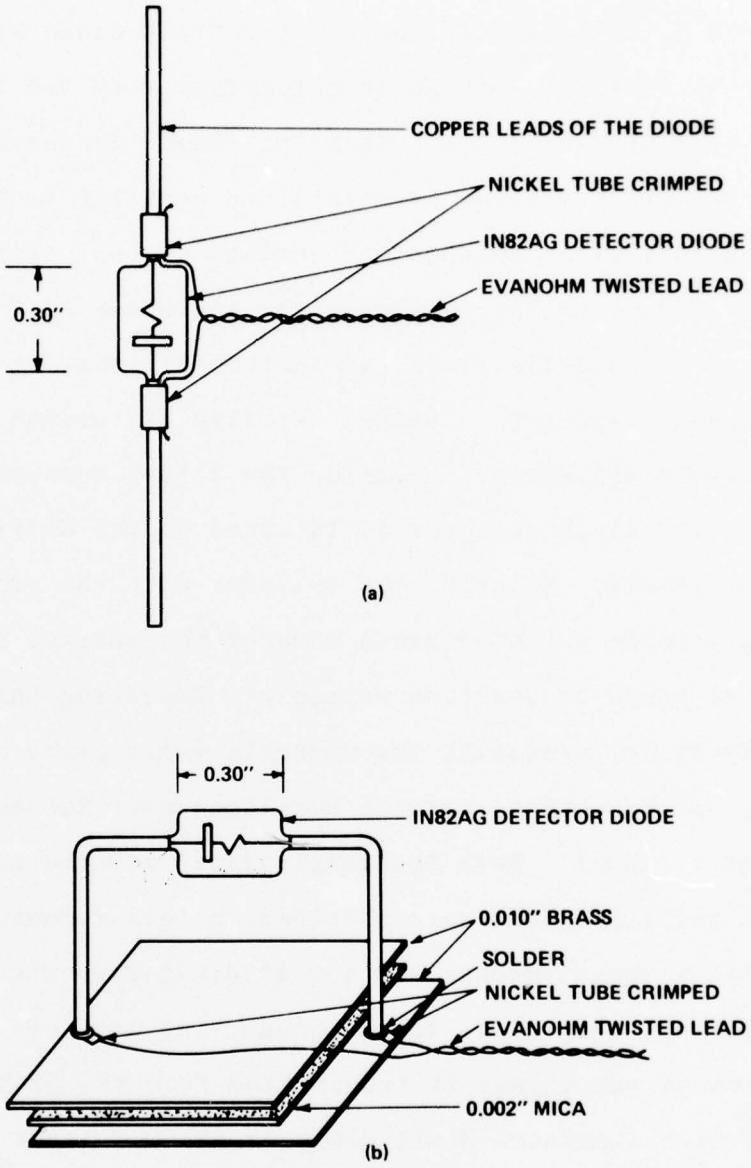

Figure 3. ELECTRIC FIELD SENSOR (a) AND SURFACE MAGNETIC FIELD (SURFACE CURRENT) SENSOR (b)

Results for the electric field along the axis of the finite length circular cylinder were obtained using the same point-contact diode as a detector in the form of a small linear dipole. Figure 3 illustrates schematically the make up of the square law electric field detector. E field measurements were made by centering the electric field detector at fixed positions on the symmetry axis of the cylinder and aligning the probe normal to that axis. In this manner we obtain measured values of $|E_r|^2/|E_o|^2$ at the axis. For E-polarized radiation measured angular scans of the radial component were taken in the direction perpendicular to the incident electric field. For H-polarized radiation the radial component of electric field was scanned azimuthally in the plane parallel to the electric field in the incident radiation.

To obtain empirical values for the surface charge density the electric field sensor was aligned along a radial direction i.e. normal to the surface of the cylinder. After the probe was aligned carefully it was fixed in position on the cylinder and the cylinder rotated about its axis. By changing the z-coordinate of the position of the radially aligned electric field detector angular scans could be made at each desired value of longitudinal position. In this manner the amplitude of the surface charge density could be mapped over the outer surface of the tube as well as over the inner surface of the hollow cylinder.

Before proceeding to the actual results obtained and a detailed discussion of their characteristics it is somewhat helpful to first

briefly consider the electronics involved in the measurement program. For the sources two oscillators were used, a Hewlett-Packard 616A for the 2-4GHz range and a Hewlett-Packard 8690B for the 1-2GHz frequency range. A Hewlett-Packard 8691A plug in unit operating in the manual mode was used in conjunction with the latter oscillator. The output signal from the probe was modulated by a 1KHz square wave from a PAR model 120 lock-in amplifier. It was also amplified by a Bogen MBT60 audio amplifier. The output of the lock-in-amplifier was fed either to the Y-axis of a Hewlett-Packard Mosely model 135 X-Y recorder or to a GE 100μa panel meter depending on application. By means of a potentiometer circuit with a Helipot the probe position was indicated by a connection outside the anechoic chamber to the rod on which the target cylinder was mounted. A motor drive was connected to the other end of the rod. In this configuration as the cylinder rotated about its axis the Helipot would permit driving along the X-axis of the recorder to establish the angle of rotation of the cylinder and probe.

III. EXPERIMENTAL RESULTS

1. Radial Component of Electric Field Along the Axis of the Hollow Cylindrical Tube.

After carefully aligning the electric field sensor to lie along the radial direction and simultaneously positioning it so as to be slightly off the cylinder axis in the radial direction the combined system of sensor and cylinder and source were similarly aligned with respect to one another. Rotating the cylinder and affixed probe then yields an angular distribution of the amplitude of the radial component of the electric field inside the tube and just ever so slightly away from the axis itself. Although there is obviously some difference from the field right at the axis the discrepancy is quite small and within the size limitations inherent in the small sensor. We nevertheless have, for all practical purposes, an extremely good measure of the field on the axis. The results obtained indicate that the amplitude of the radial field is an even function of the azimuth angle. Similar measurements at other positions along the z-axis or equivalently along the axis of the cylinder also clearly show that the amplitude of the radial field at zero radius is an even function of the longitudinal coordinate z. Recall that as shown in figure 1 the origin of the reference system of coordinates is at the precise center of the finite length cylinder. Let us first consider the experimental results for the circular tube of diameter D=7" for different lengths L. In figure 4(a) the angular scans are shown for the cylinder of

length L=7" (17.8cm). For this cylinder, and for all the others discussed in this report, the incident radiation is broadside to the cylinder and directed normal to the cylinder axis. In figure 4(a) we can see the angular distribution of the amplitude of the radial electric field at the axis for E-polarized incident radiation of wavelength λ = 23.2cm. This corresponds to $\gamma = 2\pi a/\lambda$ = 2.40 and $2h = L/\lambda$ = 0.77. Scans are shown for successive positions along the axis in intervals of z equal to one-eighth the length of the cylinder from the center, z=0, out to the end z=L/2. At z=o we found E_ρ to be zero for all values of the azimuthal variable. The remaining finite valued scans show a maximum at $\phi = 0°$ i.e. on the side away from the incident direction and a second and higher valued maximum at $\phi = 180°$ on the opposite side. For both sets of maxima the further from the center the larger the value of the maximum. Accompanying this behaviour we find that for each value of z the larger maximum occurs at $\phi = 180°$ that is on the side closest to the source of the radiation. A further significant characteristic to note is that a low lying minimum occurs for each value of z at which the scans were taken. All of these minima occur near the top and bottom of the cylindrical tube i.e. at about $\phi = \pm 90°$. Further examination of this neighborhood reveals that as we move along the axis away from the center of the tube the height of the low lying minimum rises. Also it is clear from the data that the minimum occurs at about $\phi = \pm 80°$ for $z = L/_8$ and moves gradually toward the source to just

below $\phi=\pm 90°$ for $z=L/2$. Now the curves in figure 4(a) represent the squared amplitudes of the total radial electric field at the cylinder axis. Since the incident electric field has no component that contributes to the radial electric field this field is due entirely to the response of the hollow tube to the incident radiation. Upon closer scrutiny of the scans in figure 4(a) it should be noted that they resemble rather well the functional form of $\cos^2\phi$ and hence the amplitude of the radial field as a function of azimuth goes pretty much as $\cos\phi$. Figure 4(b) shows the corresponding scans of the angular distribution at $z=0$, $z=L/4$ and $z=L/2$ for a tube of length L=6.1" (15.5cm), slightly shorter than the previous cylinder. Again we found E_ρ to be identically zero for all ϕ at $z=0$. Maxima occur at $\phi=0°$ and at $\phi=180°$. The latter are higher than the former. All maxima increase as we move along the axis toward the end of the cylindrical tube. Minima occur near $\phi=\pm 90°$. The scan at $z=L/4$ shows the minimum at about $\phi\simeq\pm 87°$ and that at $z=L/2$ locates the minimum at just about $\phi=\pm 90°$. The general characteristics displayed by $|E_\rho|$ for the L=6.1" cylinder are very nearly those of the L=7" cylinder. In figure 5(a) we show the empirical results for the amplitude of the radial electric field along the axis of an L=4.875" (13.3cm) tube. Again the radial electric field is identically zero at $z=0$ for all values of ϕ. The same behaviour with ϕ as in figure 4 can be seen for scans at increasing z along the axis. At this point we can clearly observe a decrease in the maximum of the amplitude of the radial component of the electric field on the axis

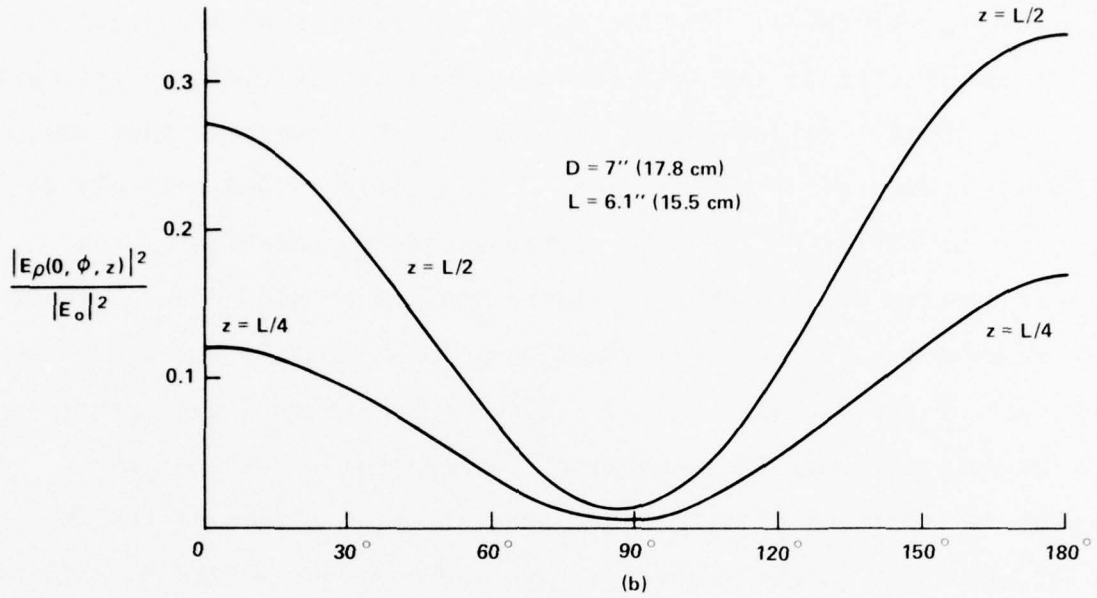

(b)

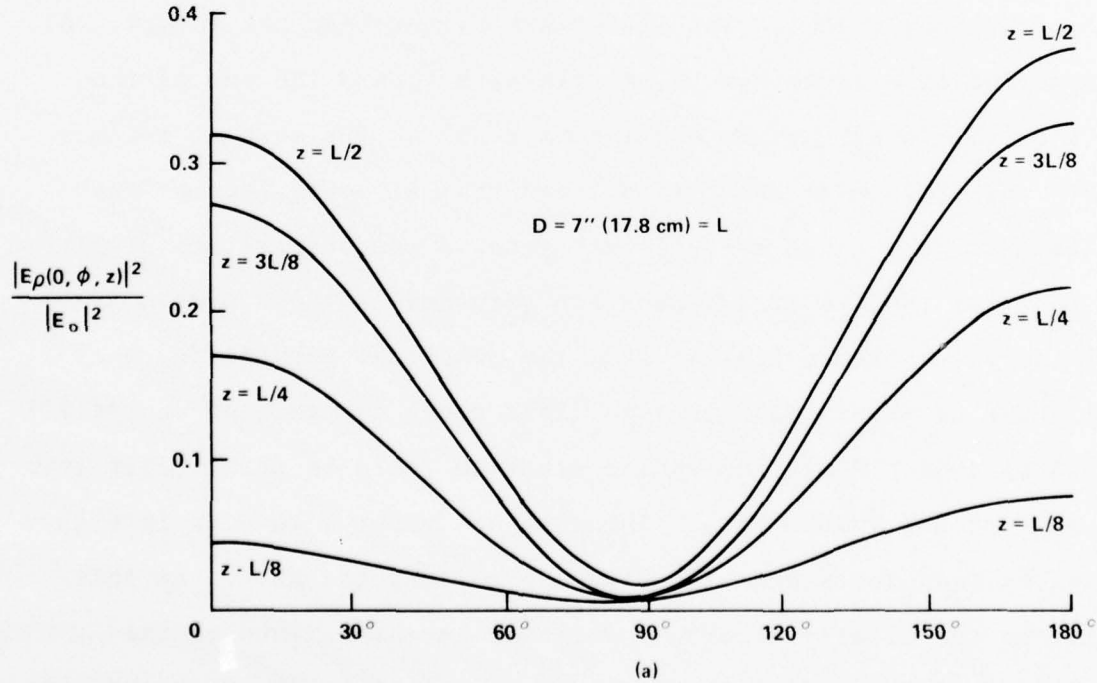

(a)

FIG. 4 ANGULAR DISTRIBUTION OF RADIAL COMPONENT OF E-FIELD ALONG THE AXIS OF A CIRCULAR TUBE OF VARIABLE LENGTH. INCIDENT RADIATION IS E-POLARIZED AND DIRECTED BROADSIDE

at the ends of the tube as the tube length is decreased. This occurs at both $\phi=0°$ and 180°. Figure 5(b) again shows a considerable decrease in the maxima at $\phi=0°$ and $\phi=180°$ as the tube is further shortened to a length of 2.94" (7.77cm). At $z=0$ we again observed that the angular distribution of the radial component of electric field vanished for all angles at the axis. The tube is now less than half as long as its diameter and we must begin now to think of the diffracting target more as a wide ring than as a hollow cylinder. While we again observe that the larger amplitude maximum occurs at $\phi=180°$ compared to that at $\phi=0°$ and that both maxima increase as we move towards the ends of the tube or ring as we noted before for the longer cylinders we now observe a significant change in character for the radial electric field at the axis. The first obvious deviation from the previously noted behaviour is the much lower maxima at $\phi=0°$ relative to those at $\phi=180°$. In addition we find the minimum is much less defined at $z=L/4$ lying near $\phi=\pm60°$. For $z=L/2$ the minimum is still well defined but lies at about $\phi=\pm70°$. If we shorten the tube further to L=1.5" (3.8cm) which is only about one fifth the diameter we clearly have a ring rather than a cylinder as the target. For this case shown in figure 5(c) we have $\gamma=2\pi a/\lambda = 2.40$ for the circumference to wavelength ratio and $2h/\lambda = L/\lambda = 0.16$ for the length to wavelength ratio. This effective change in the geometric properties is reflected in the experimentally observed radial electric field distributions at the axis. At z=o the radial electric field is again zero for all angles. Clearly

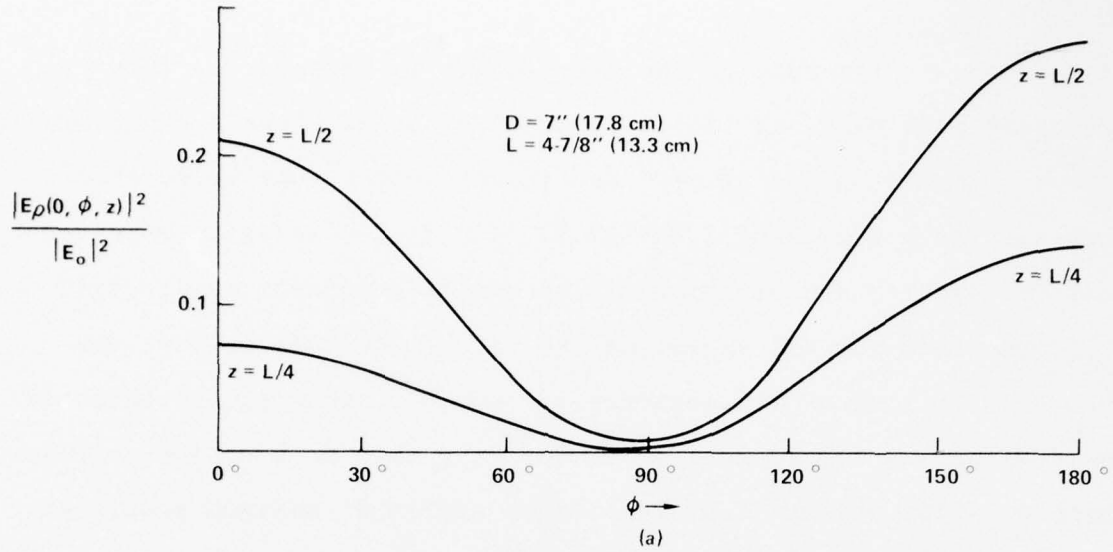

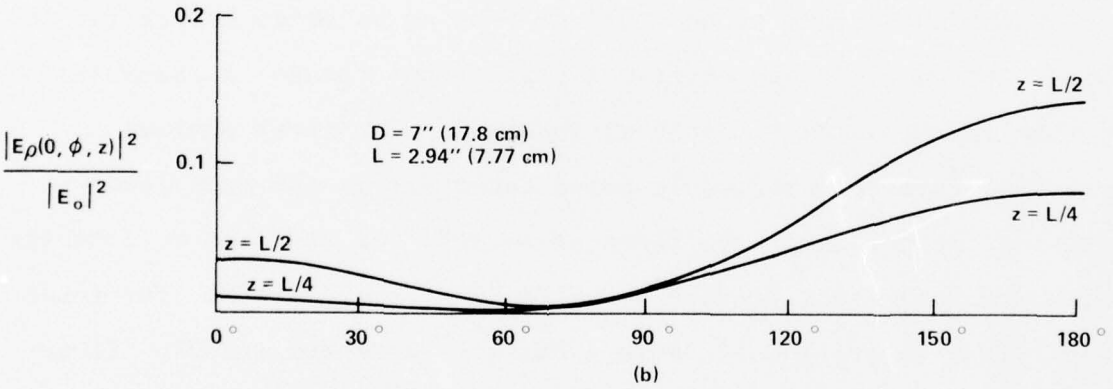

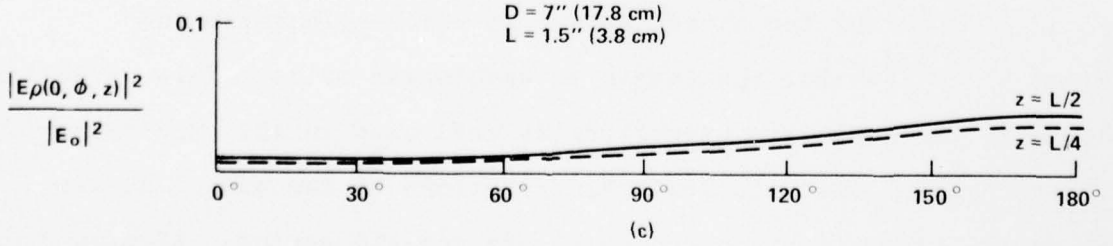

FIG. 5 ANGULAR DISTRIBUTION OF RADIAL ELECTRIC FIELD ALONG THE AXIS OF CIRCULAR CYLINDER, DIAMETER D = 7" (17.78 cm), LENGTH L AND γ = 2.40 AT E-POLARIZATION.

maxima occur at $\phi=180°$ that at $z=L/2$ is only slightly higher than the peak at $z=L/4$. At $\phi=0°$ on the other hand there occur just barely perceptible maxima the one at $z=L/2$ lies just above the one for $z=L/4$. Actually the entire distributions are quite flat. This is especially true near $\phi=0°$. Minima are also just barely discernible. At $z=L/4$ the minimum occurs at about $\phi=\pm 20°$ and for $z=L/2$ slight minima lie at about $\phi=\pm 25°$. Figures 4 and 5 reveal experimentally the characteristics of transition from a diffracting short cylindrical tube to a diffracting finite ring or short circular collar for fixed diameter and fixed wavelength at E-polarization.

For emphasis we repeat that although there is no radial component of electric field in the E-polarized incident radiation we do indeed find that the finite length target cylinder has a radial electric field in its interior.

Consider next the experimentally determined distribution of the radial component of electric field on the axis of the finite cylinder for the same circumference to wavelength ratio $\gamma=2.40$ but for H-polarized incident radiation. In figure 6 we show the results obtained for the azimuthal distribution with the electric field probe at the center of the cylinder axis. Measured results are shown for lengths of cylinder that coincide with the earlier lengths used in the E-polarization study (except L=7" which is shown in figure 7). The behaviour at H-polarization is similar and complementary to that obtained for the E-polarized incident radiation. At $z=0$ we observe for all cases of length L that maxima occur at

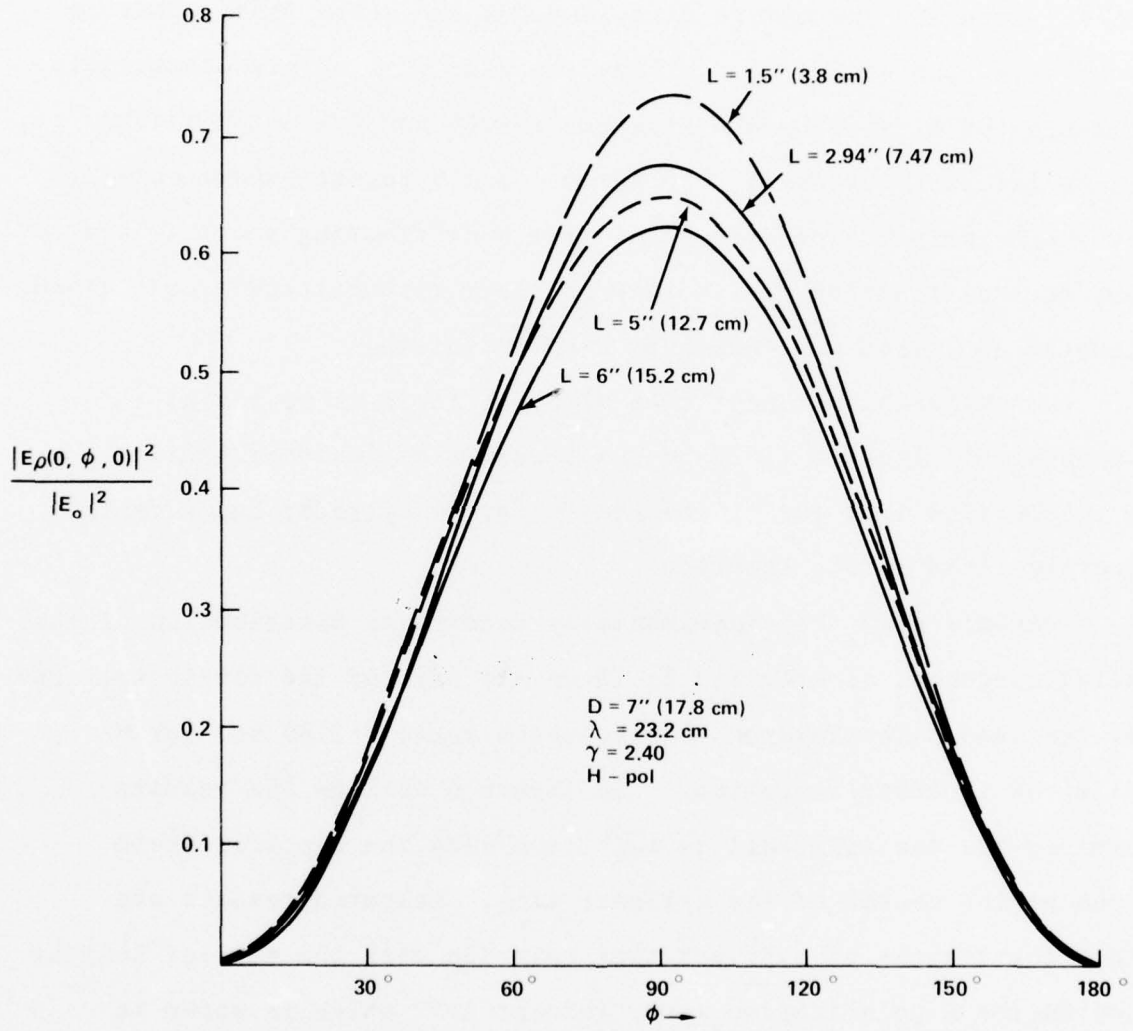

FIG. 6 ANGULAR DISTRIBUTION OF THE RADIAL COMPONENT OF THE ELECTRIC FIELD AT THE CENTER OF THE OPEN ENDED CIRCULAR TUBE. THE DEPENDENCE ON CYLINDER LENGTH L IS SHOWN FOR $2\pi a/\lambda = 2.40$ AND NORMAL BROADSIDE INCIDENCE.

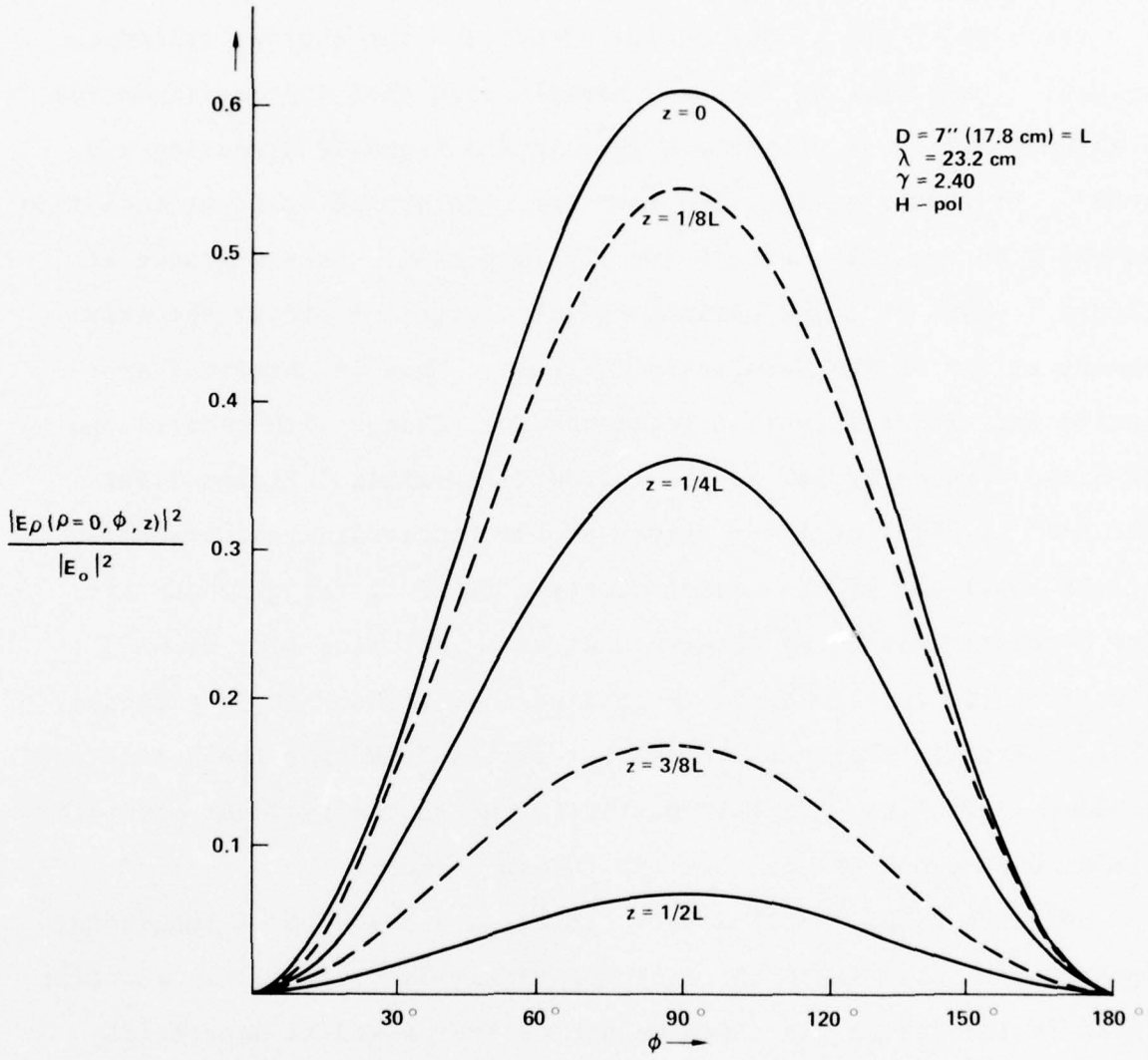

FIG. 7 ANGULAR DISTRIBUTION OF THE RADIAL COMPONENT OF THE E-FIELD ALONG THE AXIS OF AN OPEN ENDED CIRCULAR TUBE OF LENGTH L AND DIAMETER D. RADIATION IS H-POLARIZED AND INCIDENT BROADSIDE

about the top and bottom of the cylinder i.e. $\phi=\pm 90°$, and minima are found at the forward $\phi=0°$, and backward $\phi=180°$ azimuths. These minima are actually zero amplitudes. Furthermore as can be seen in figures 6 and 7 the higher maxima occurs for the shorter cylinder length. Inspection of figure 6 reveals also that the amplitude for a given length L is slightly higher in the backward direction i.e. $\phi>90°$. It should be recalled that for E-polarized incident radiation we had $E_\rho \equiv 0$ for all ϕ at $z=0$ for all lengths L. Just a glance at figure 7 shows that the maximum radial electric field at the axis occurs at $z=0$ in the H-polarization case. Thus we observe that maxima and minima azimuthal locations interchange with interchange of E and H polarization in the incident radiation. Figure 7 for the L=7" (17.8cm) cylinder, gives us the longitudinal distribution of the amplitude of the radial electric field at the cylinder axis for H-polarization. We observe that as z increases i.e. as we move from the center toward the end of the cylinder $|E_\rho|$ decreases. This is exactly the opposite characteristic found for the E-polarized incident radiation. This is partially due to the incident electric field being primarily parallel to the tube ends.

Figures 6 and 7 follow very closely a $\sin^2\phi$ type of functional dependence. Also since the incident radiation possesses an electric field in the radial direction we are not surprised to detect its effect in the interior of the open ended tube. In figure 8 we present a comparison of the distributions of the peak amplitude of radial electric field along the axis of a D=7" (17.78cm) = L

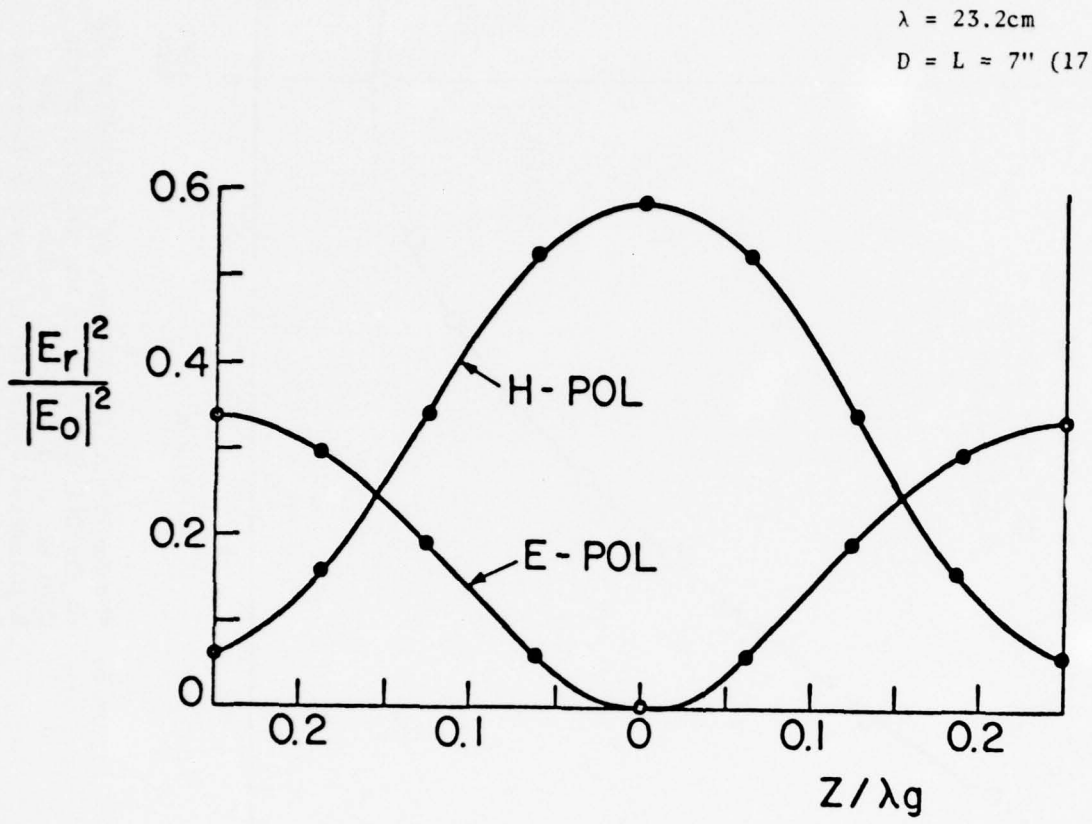

Figure 8. Radial Component of Electric Field Along the Cylinder Axis, $|E_r| = |E_y|$ for H-polarization and $|E_r| = |E_x|$ for E-polarization. Hollow tube of Diameter D equal to the Length L = 7" (17.8 cm)

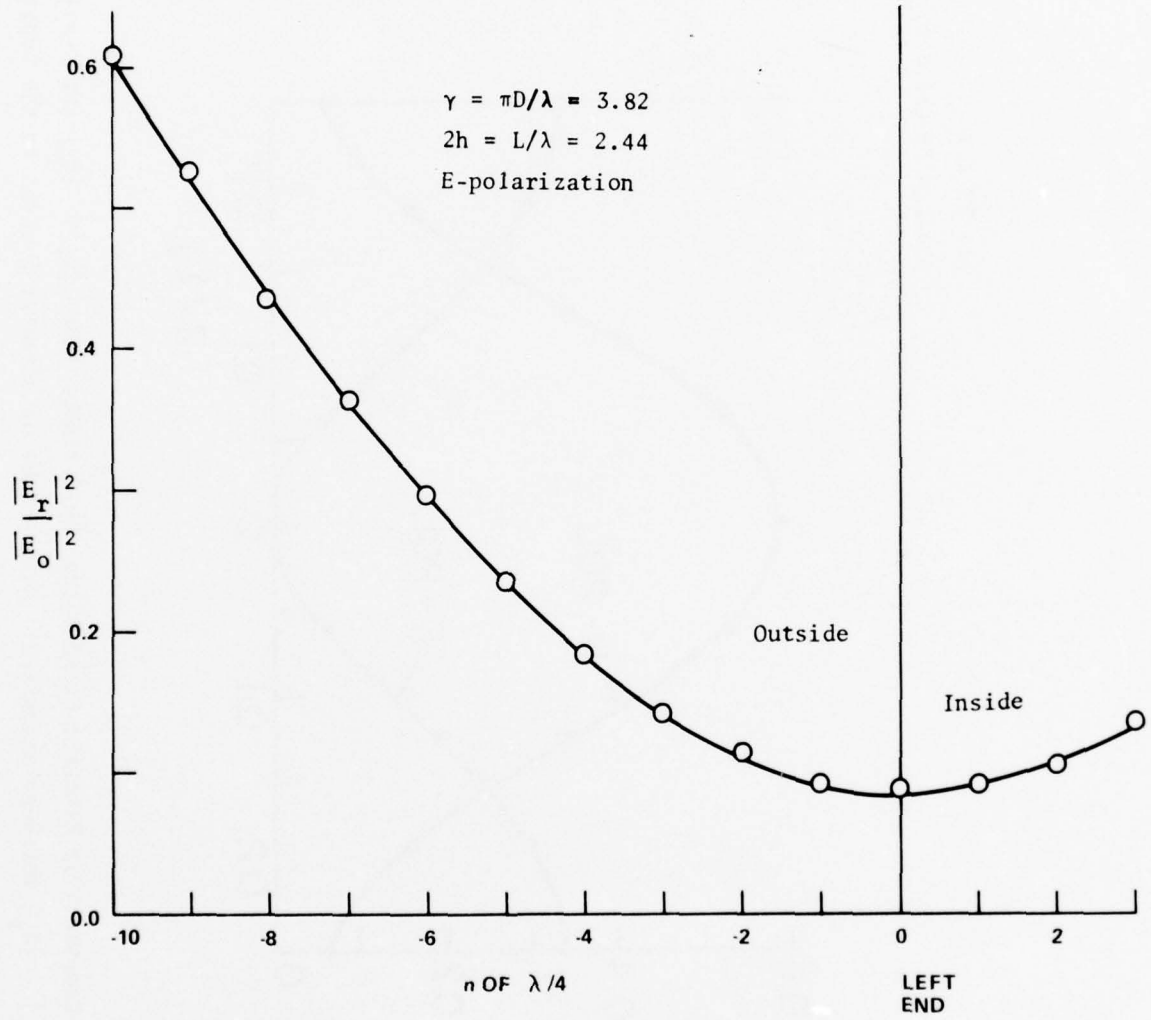

Figure 9. The Radial or X- Component of Electric Field on the Cylinder Axis in the Vicinity of the Open End of a Hollow Circular Tube. The E-polarized radiation is normally incident broadside on a D= 6 1/8" (15.5cm), L = 12" (30.5cm) cylinder.

circular open ended cylinder for the same circumference to wavelength ratio γ=2.40 of the incident radiation at E and at H-polarization. The value found experimentally for $\lambda\hat{g}$ was precisely equal to the length L=7" (17.78cm). Figure 9 shows the corroborating results obtained for the measured radial electric field on the tube axis inside near the end of the cylinder and outside on the axis for the case of H-polarized incident radiation. We thus appear to have a standing wave pattern that goes as $\cos\phi$ and $\cos(\pi z/h)$ for E-polarization and varies as $\sin\phi$ and roughly $\sin(\pi z/h)$ for H-polarization for the same cylinder irradiated with λ=23.2cm radiation. It should be obvious that in view of the measured distributions the edges play a significant role in the diffraction characteristics of the finite open tube. They are clearly responsible for the occurrence of a field distribution in the interior other than that of the TM_{01} mode that one would have anticipated for the E-polarization case with γ=2.40.

2. Surface Charge Density on the Interior Wall of the Hollow Cylindrical Tube.

Measurement of the surface charge density over the inner wall was achieved by carefully aligning the electric field probe to lie along a radial line and just inward of the interior wall. This of course also requires a careful alignment of cylinder and source with the probe in place. Rotation of the system with the probe fixed relative to the tube then produces an angular scan at the fixed value of z. Repeating this procedure for different values

of z results in the distribution of surface charge density over the entire interior wall of the open ended tube. Obviously we cannot measure the normal component precisely at the wall due to the finite size of the real electric field detector used to make the measurements. Nevertheless the fact that the probe is quite small compared to the wavelength still yields an accurate result for the measured amplitude of surface charge density distribution on the conducting wall.

As stated earlier measurements of surface charge density were made only for the case of H-polarized normally incident radiation.

Consider first the measured results obtained for the open ended tube of diameter D=7" (17.78cm) = length L. The incident radiation has wavelength λ=23.2cm which means once again the circumference to wavelength ratio is γ=2.40. Figure 10 shows the angular scans obtained at several distances along the tube. Until we get very close to the ends of the tube we find that the amplitude of the surface charge density has a single maximum at about $\phi=\pm 90°$, which is slightly shifted toward the source. There are also minima at $\phi=0°$, the forward direction, and $\phi=180°$, the backward direction. This is consistent with the z-dependence found at the symmetry axis for the amplitude of the radial electric field component as shown in figures 7 and 8, for the same tube and same incident radiation. On the inside wall we find that the surface charge density decreases as we move from the center of the wall

toward the tube ends. There is one departure from this overall behaviour that was observed at z=2.7". At this value of z we are at 0.3" from the end and unfortunately this distance is comparable to the probe dimensions. Consequently we should not be surprised to discover some deviation in the measured behaviour of the surface charge density. This probably accounts for the minimum observed for this location along z in the neighborhood of $\phi=\pm 90°$ where the probe is aligned pretty much parallel to the incident electric field. The angular scans on the interior walls seem to corroborate the angular scans made along the tube axis. It should be pointed out that the surface charge measurements were carried out about one year later than the field measurements along the axis. One can therefore safely conclude that at the axis the radial field goes as $\sin\phi$ for $\gamma=2.40$ for this tube and the surface charge density does likewise on the inside wall of this open ended circular cylinder.

In figure 11 we show the results obtained for the measured amplitude distribution of surface charge density over the inner wall for the 12" (30.4cm) long hollow tube of inside diameter 6" (15.2cm) with both ends open. The incident radiation of wavelength $\lambda=12.5$cm is also H-polarized and directed normal and broadside to the cylinder. Since figure 11 gives the amplitude squared we observe that the ϕ dependence of the charge density on the inner surface is reasonably well described by the function $\sin 2\phi$. Note that the circumference to wavelength ratio inside is $\gamma_{int.}=3.80$. The radial

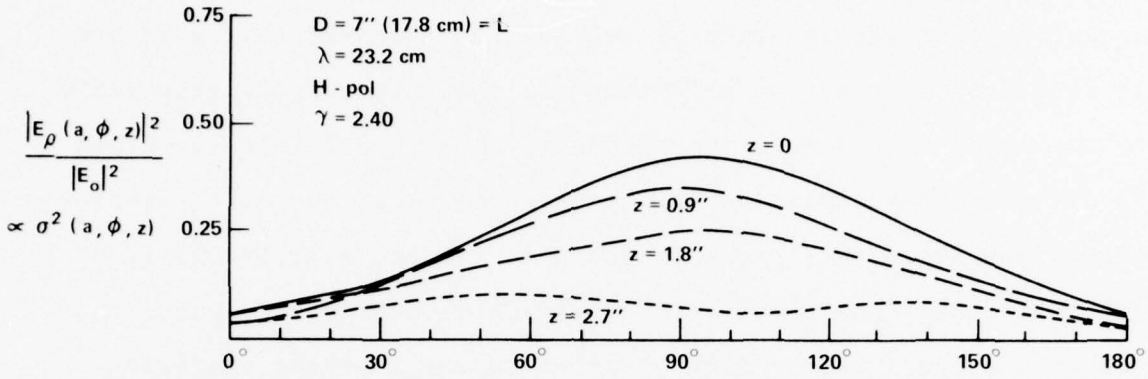

FIG. 10 ANGULAR DISTRIBUTION OF CHARGE DENSITY ALONG INSIDE SURFACE OF OPEN ENDED CIRCULAR TUBE FOR D = 7" (17.8 cm) = L. H-POLARIZED NORMAL BROADSIDE INCIDENT RADIATION OF λ = 23.2 cm

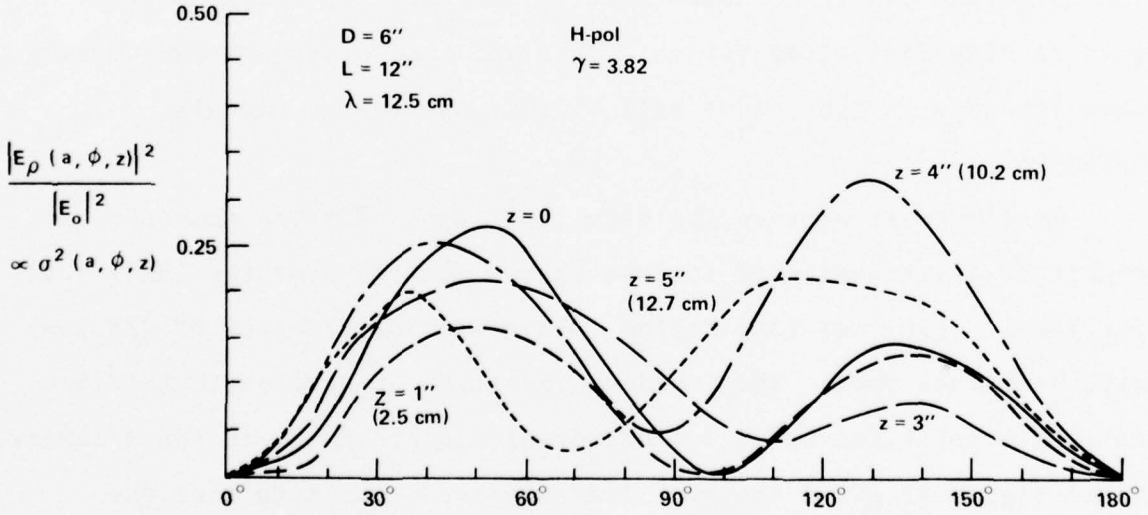

FIG. 11 ANGULAR DISTRIBUTION OF CHARGE DENSITY ALONG INSIDE SURFACE OF OPEN ENDED CIRCULAR TUBE OF 6" (15.2 cm) DIAMETER AND 12" (30.4 cm) LENGTH. H-POLARIZED NORMAL BROADSIDE INCIDENT RADIATION OF λ = 12.5 cm

electric field at the inside wall clearly indicates the presence of a higher mode. It is somewhat interesting to observe the behaviour of the ϕ dependence as we move from z=0 towards the open ends of the tube. At z=0 we have nulls at ϕ=0° and ϕ=180° but we also find another at about ϕ=±110°. A maximum occurs at about ϕ=±50° and is about twice as high as that occurring at ϕ=135°. As we move to z=1" (2.5cm) the center null moves closer to ϕ=±90° and the maximum in the more forward direction drops to lie only slightly higher than the maximum closer to the source. At z = 3" = $\frac{L}{4}$ the characteristics return closer to those for z=0 although both maxima lie lower than those for z=0. In addition there is now a low lying minimum at ϕ=±110° rather than a definite null. Moving further out to z=4" we find again a low lying minimum at about ϕ=±85° rather than a null. Also we have a high maximum at ϕ=±130° and a lower maximum near ϕ=±40°. A reversal in the locations of the higher maxima occurs as we move towards the open ends. At z=5" even further out toward the end the intermediate minimum lies lower and shifts further forward to about ϕ=±67°. Simultaneously the two maxima decrease in height and are about equal to each other lying at ϕ=±35° and ϕ=±110°. Overall there appears to be a general decrease in surface charge density as we move away from the center followed by a significant increase near the end and another drop off thereafter. Although we did not measure the radial component of electric field along the axis for this case it is probably safe to speculate that it behaves pretty much as the surface charge density on the inner wall.

We point out that the results presented above appear to be the first such data to be published and hence there is nothing available to compare them with as yet.

3. Charge Density on the Outside Surface of the Hollow Open Ended Tube.

The first straightforward comparison of the measurements with a theory can be made for the charge density on the outside surface of the open ended tube. Unfortunately the only available data one can compare the measurements to are the analytic predictions for the induced surface charge density on an infinite circular cylinder. Basically then we are limited to assessing how well the physical quantity in question for a finite length, hollow, open ended tube can be approximated by the well known infinite cylinder solutions. This is by no means an insignificant question itself.

Figure 12 gives the azimuthal distribution of the measured amplitude of the charge density on the outer surface of the open-ended hollow cylinder of diameter D=6" (15.2cm) and length L=12" (30.5cm). The cylinder is irradiated at normal incidence by an H-polarized monochromatic plane wave of wavelength λ=12.5cm. The pertinent parameters are circumference to wavelength ratio γ=3.82, and length to wavelength ratio $L/\lambda = 2h/\lambda = 2.44$. As can be seen by inspection of figure 12 the angular scans of the surface charge density induced on the outer wall were made around the center and in steps of 1" towards the tube ends. Note that the cylinder is just short of being 5/2 wavelengths long. Let us first discuss the

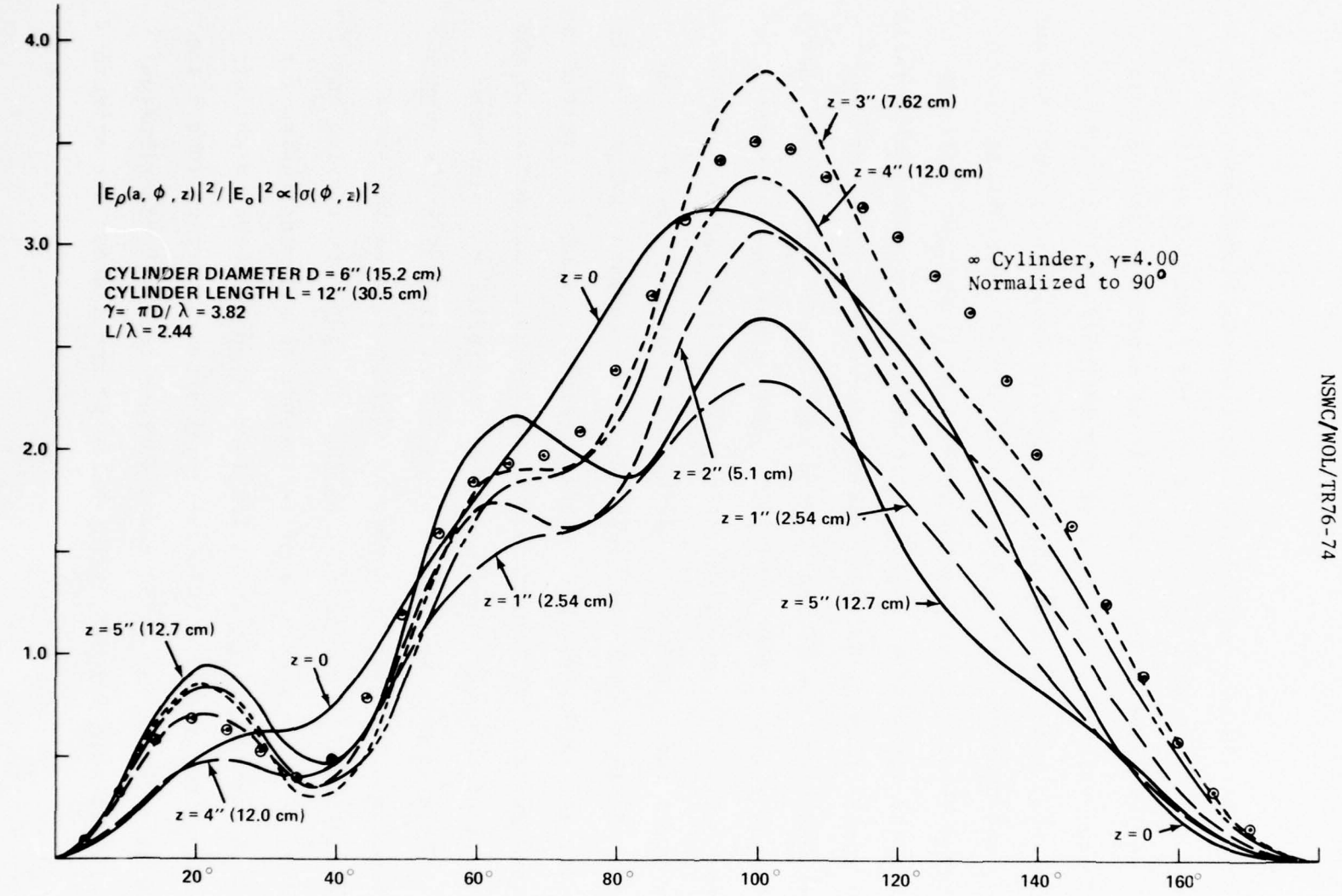

FIG12 ANGULAR DISTRIBUTION OF THE SURFACE CHARGE DENSITY ON THE OUTSIDE OF AN OPEN ENDED TUBE IRRADIATED BY λ = 12.5 cm H-POLARIZED RADIATION AT BROADSIDE INCIDENCE

experimental results. Around the center of the finite tube, $z=0$, we first observe a null at $\phi=0°$ i.e. in the forward direction. At $\phi=\pm33°$ an inflexion point appears. As we proceed further around toward the source the amplitude of the charge density continues to monotonically rise, passing through another inflexion point at about $\phi=\pm70°$, and achieves its peak height at $\phi=\pm93°$. Continuing around the charge density drops passing through still another inflexion point in the vicinity of $\phi=\pm125°$. Thereafter it monotonically falls off to vanish finally on the backside toward the source, at $\phi=\pi$. The next angular scan of the squared amplitude of the surface charge density was taken at z=1" (this is a shift along the z-direction of about 0.2λ). The amplitude hardly varies from that around the center until the neighborhood of the inflexion point at $\phi=33°$ is reached. At that point the amplitude of the surface charge density drops for z=1" and a clearly defined minimum is found rather than an inflexion point. The amplitude then rises and almost parallels the $z=0$ distribution until the vicinity of the inflexion point near $\phi=70°$. Here we observe again a point of inflexion for the z=1" distribution. This time however the distribution of the surface charge amplitude is not as flat as that for $z=0$. Continuing on around we find the squared amplitude monotonically increasing for z=1" to a maximum height about 15% lower than the peak height of the central curve. Also the lower peak appears further toward the source at $\phi=\pm100°$. As ϕ increases further the z=1" distribution follows that seen for $z=0$, lying below it until about the azimuth

$\phi=\pm 152°$ whereupon it still follows the z=0 curve but sits just slightly above it until it vanishes at $\phi=\pi$ also. Clearly the angular distribution for z=1" displays an increase in structural detail over that for z=0. This sharpening of structural detail is further enhanced by scanning around the cylinder at z=2" (here we are about 0.4λ from the central scan). As expected the distribution starts at zero at $\phi=0°$, it then increases steadily to a peak about 1/3 higher than that for z=1", occurring at $\phi=\pm 20°$ just before the latter peak and drops to a slightly lower minimum at about the same azimuth as the z=1" curve. For z=2" the inflexion point observed for smaller z becomes clearly resolved into a minimum located at $\phi=\pm 75°$. This, of course, is accompanied by a maximum at $\phi=\pm 62°$ for the z=2" curve. Over the range of azimuth from about $\phi=45°$ to the subsequent minimum in the z=2" distribution the latter lies above the z=1" curve. As ϕ increases further the z=2" curve increases and peaks at about the same azimuthal position as the z=1" distribution. There the former is about 1/3 higher than the latter. Thereafter the z=2" curve behaves pretty much like the z=1" curve for the surface charge density-always lying above it though-and also vanishes at $\phi=\pi$. As z increases to 3" (7.6cm)- a shift of about 0.6λ from the central scan-we note that the experimental angular distribution found is very much similar to the surface charge density distribution at z=2". Starting from a null in the forward direction we see a monotonic increase to a maximum at $\phi=\pm 21°$. This is almost coincident with the azimuthal position of the corresponding maximum for z=2". At this maximum the height of the z=3"

maximum is about 25% higher than the corresponding maximum measured for the z=2" squared amplitude of the surface charge density. We find with increasing ϕ a smoothly decreasing amplitude of surface charge density until a minimum is reached at $\phi=\pm 37°$. This is just about where the minima occur for the z=1" and z=2" scans of surface charge density. The z=3" scan lies above both of these latter curves until at about $\phi=\pm 31°$ it falls below the z=2" scan and then at $\phi \tilde{=} 32.5°$ it drops below the z=1" scan of the surface charge. The z=3" minimum is the lowest one observed in the set of measurements taken along the hollow tube. Until $\phi=\pm 48°$ the z=3" curve still remains lowest. It exceeds the z=1" curve at that point remaining above it thereafter. At $\phi=\pm 55°$ it catches up with the z=2" scan and thereafter remains above it. The measured data as shown in figure 12 indicate that at z=3" the squared amplitude of the surface charge density increases steadily from $\phi=\pm 37°$ to another maximum at $\phi=\pm 55°$. Here the height of the z=3" curve is only about 10% higher than the observed value at z=2" for that azimuthal location. Further increasing ϕ we note gives rise to a very slight decrease to a very shallow minimum at $\phi=\pm 70°$. It would thus seem that the process of sharpening of the structural detail in this neighborhood with increasing longitudinal position has been significantly reduced. It should be noted that the longitudinal position of the angular scan is now about $\lambda/2$ from the z=0 scan. Continuing with the surface charge density variation with increasing ϕ at z=3" we observe a relatively rapid but smooth increase in the squared amplitude of surface charge density. This characteristic continues until a

maximum at $\phi=\pm 100°$ is attained. Note that this is an absolute maximum found for all values of longitudinal position z. At this azimuthal position the height of the z=3" scan is 25% higher than that for z=0 or z=2" and about 50% higher than that for z=1". With further increase in the azimuthal variable ϕ we find the z=3" angular scan closely resembles the distribution found for z=0, 1" and 2", lying above all three until the common null is reached at $\phi=\pi$ on the incident side. There is one further interesting characteristic revealed by the z=3" angular distribution. It shows rather clearly the occurrence of an inflection point in the angular distribution on the side facing the source. This can be seen in figure 12 to lie at $\phi=\pm 130°$ for z=3". The measurements at z=4" (about $\lambda/2$ from the tube end) show that the angular distribution of the amplitude of the surface charge density is remarkably like the observed z=3" scan. From the null on the shadow side at $\phi=0°$ to the first maximum at $\phi=\pm 22°$ the z=4" distribution lies just below and quite close in fact to the z=3" distribution. Recall that the latter has its maximum in this region at $\phi=\pm 21°$. Over the range from $\phi \cong 21.5°$ to $\phi \cong 44°$ the z=4" curve lies above the z=3" measurements. This constitutes the only range of azimuth where the z=4" distribution lies above the z=3" measured results. Upon inspection of figure 12 we find a minimum has been observed at $\phi=\pm 37°$ for the empirical distribution at z=4". This is nearly coincident with the azimuthal position detected for the minimum of the z=3" distribution. As ϕ continues to increase we note that the

measured results for z=4" continuously increase. From ϕ=44° on around the z=4" data lie quite close to but clearly below the z=3" results obtained for the squared amplitude of the surface charge density. We further observe that for z=4" we do not find a minimum in the ϕ=±70° region. Rather an inflection point is present at about ϕ=±68°. Still increasing ϕ we observe that the z=4" results are very close qualitatively in character to the z=3" measurements. A maximum is reached at ϕ=±100°. The height at this maximum is about midway between that for z=3" and z=2". Thereafter as ϕ increases the z=4" distribution runs almost parallel to that for z=3" and roughly speaking is midway between the z=2" and z=3" surface charge distributions meeting both at the null at $\phi=\pi$. The inflection point on the illuminated side at z=4" is more pronounced and occurs at approximately ϕ=±129° very close to the location of the corresponding inflection point for z=3". It would appear that for $z<5" \approx \lambda$ the ends of the finite length hollow tube do have an effect on the outer surface charge distribution. Nevertheless over this length of the tube that effect is not terribly drastic either on the shadow side or the illuminated side. As we consider the angular scan at larger distances from the center and hence get even closer to the tube ends we do indeed find as expected a much more emphasized effect due to the finiteness of the cylindrical tube. This is quite evident in figure 12 for the z=5" azimuthal scan (we are now about 0.2λ from the tube end and simultaneously about one wavelength from the central circle of scan). Again the z=5" scan starts with a null at ϕ=0°.

It then rises steadily to a maximum at $\phi=22°$ lying above all the other scans for smaller z values. Only the amplitude on the central scan at z=0 exceeds the z=5" data from $\phi=31.5°$ to $\phi=51.5°$. Apparently the presence of the clearly defined maximum in this neighborhood of ϕ is a consequence of the finite length of the tube, which is more evident the further one gets from the center. Increasing ϕ still further the z=5" distribution falls steadily to a clearly defined minimum at $\phi \tilde{=} 40$. Over this range the z=5" distribution still lies above all the others. Again it would appear that due to the existence of the ends of the tube we find a clearly defined minimum. From $\phi=40°$ to $\phi=45°$ the measured amplitude of the surface charge density for z=5" lies below but nearly coincident with the z=1" distribution but still is above all but the z=0 scans. The z=5" agains oscillates back to lie above the z=0 scan at $\phi=\pm41.5°$ and remains above it until the azimuthal position $\phi=\pm68°$ is reached. From this point on it remains below until well around on the illuminated side at $\phi=\pm152°$ where it again climbs above the z=0 scan and remains there as they both decrease to the null at $\phi=\pi$. For z=5" we find another clearly defined maximum displayed at $\phi \tilde{=} \pm 66°$ and a clear minimum somewhat further around at $\phi \tilde{=} \pm 81°$. Again it appears that this well defined pair of a maximum and minimum result from the relative proximity of the tube ends. Until $\phi \tilde{=} \pm 75°$ the z=5" surface charge distribution has a larger amplitude than all but the z=0 scan. From $\phi \tilde{=} \pm 75°$ to $\phi=\pm81.5°$ the amplitude at z=3" and at z=4" become considerably larger than that for z=5".

At $\phi=\pm 81.5$ the z=2" joins the others above the z=5" distribution and these three scans remain higher in amplitude until the null at $\phi=\pi$. The z=5" distribution also has a well defined maximum at $\phi=\pm 100°$. This is common for all the z>o scans. At larger azimuths $\phi\tilde{=}\pm 114°$ and $\phi\tilde{=}\pm 141°$ the z=5" distribution reveals the existence of two inflection points. This is another indication of the complexity of the structural details induced in the surface charge distribution by the proximity of the ends of the finite tube. The oscillatory nature of the z=5" scan relative to the z=0 scan is also characteristic of the relative behaviour with respect to the z=1" scan. At $\phi\tilde{=}\pm 84.5°$ the z=5" distribution nearly coincides with the z=1" scan it then rises significantly higher and eventually crosses the z=1" distribution at about $\phi=\pm 114°$. It remains lower until ϕ increases to about $\phi=\pm 152°$ whereupon it climbs back above and then remains above until the null appears at $\phi=\pi$.

We have included in figure 12 the theoretical predictions for the squared amplitude of the surface charge density distribution around an infinite cylinder for $\gamma=4.0$. The distribution is very close to that for precisely $\gamma=3.82$. In fact the difference is for all practical purposes negligible. Furthermore for qualitative comparison purposes we have normalized the infinite cylinder predictions so that they coincide with the experimental results at z=0 and $\phi=\pm 90°$. Recalling that for the infinite cylinder there is no dependence on the longitudinal coordinate z we can immediately draw two conclusions. The finite length tube displays considerably

more oscillatory behaviour in its angular distribution of its surface charge density. This behaviour is more enhanced as the tube ends are approached. Secondly except quite close to the tube ends the linear amplitude of the surface charge density is quite remarkably well described by the infinite cylinder predictions when the latter are appropriately normalized. It would then seem that for a reasonably fat cylinder whose length is several wavelengths long the infinite cylindrical theory describes rather well (except for the small details) the amplitude of the surface charge density for most practical purposes. This holds out to about $\lambda/4$ from the tube ends if the theory is normalized to a measured value somewhere along the central circle and on the shadow side. Of course we are considering H-polarized incident radiation here. For E-polarized incident radiation the infinite cylinder is less accurate as we have found experimentally and shall report on in subsequent reports. This will indeed be the case unless the ratio L/λ is considerably larger than the case discussed above.

We next consider an experimental study for a specific case where $L/\lambda \tilde{<} 1$.

We show in figure 13 the experimentally determined distribution of the squared amplitude of the surface charge density around the circumference of a tube of diameter D=7" (17.8cm) and of length L=7". These measured angular distributions are displayed for circles at different locations along the cylinder axis. The cylinder was irradiated at normal broadside incidence with a monochromatic plane

wave of wavelength λ=23.3cm polarized perpendicular to the axis of the tube. For this case the relevant parameters are the ratio of the circumference to wavelength $\gamma=\pi D/\lambda=2.40$ and the ratio of the tube length to wavelength $2h/\lambda=L/\lambda=0.8$. We have basically a cylinder that is just under a wavelength long and is moderately thick.

Again the only available theoretical results that can be utilized for comparison are those for the surface charge density induced on an infinite circular cylinder. Just as before we are limited to assessing how well the infinite cylinder predictions describe the surface charge density on the lateral surface of the finite circular tube.

Consider first the scan around the outside of the cylinder at the center of the tube i.e. at z=0. This distribution should most closely approximate the infinite cylinder behaviour. What is actually observed is a rapid increase in amplitude from the null at $\phi=0°$, i.e. on the side away from the source, to a maximum at about $\phi=\pm32°$. This is followed by a steady drop to a minimum at half the maximum amplitude at about $\phi=\pm58°$, another rapid steady rise to a second higher maximum at $\phi=\pm90°$. The amplitude here is about 50% higher than at the first maximum. Further around the tube on the side toward the source we observe a steady decrease in amplitude passing through an inflection point in the vicinity of $\phi=\pm123°$ and continuing down to vanish at $\phi=\pi$. If the scan is taken away from the center at z=0.9" (2.3cm) where $z/\lambda\approx 0.1$ we find not too surprisingly almost a repeat of the central scan. What can be discerned

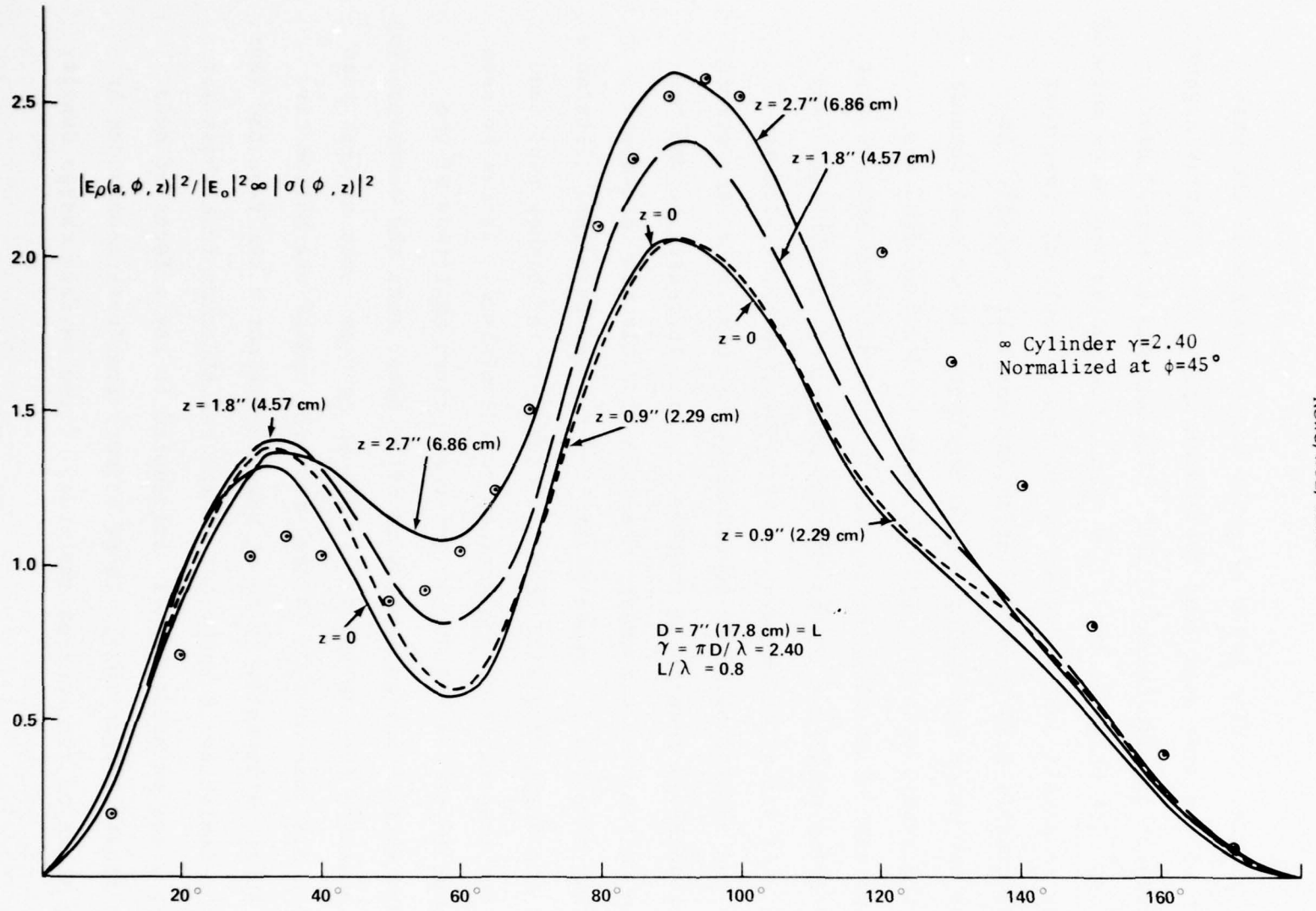

FIG13 ANGULAR DISTRIBUTION OF SURFACE CHARGE DENSITY ON THE OUTSIDE OF AN OPEN TUBE IRRADIATED BY λ = 23.3 cm H-POLARIZED RADIATION AT BROADSIDE INCIDENCE

in the plotted results are a slightly higher maximum at the same azimuth on the side away from the source and a very slightly higher amplitude at the minimum at $\phi=\pm 58°$. The maximum at $\phi=\pm 90°$ nearly coincides with that for the z = 0 scan. Continuing around we noticed a somewhat significant increase in the z=0.9" amplitude over that for the central scan from the inflection point at $\phi=\pm 123°$. At $\phi=\pi$ the two scans eventually vanish together. As we move further along the z-axis to z=1.8" (4.6cm) where $z/\lambda \approx 0.2$ we find the measured scan of surface charge density is nearly the same as that observed for smaller z values for the ranges of azimuth $\phi \lesssim 35°$ and $\phi \gtrsim 140°$. At z=1.8" we observe the first maximum lying slightly higher and shifted slightly toward larger ϕ relative to the corresponding observed results at smaller z. As ϕ increases beyond the maximum we again note a steady decrease to a minimum coincident with that observed for scans of smaller z. The principal difference out at the larger distance from the center is the higher amplitude found for the scan from the maximum to the minimum. As can be seen in figure 13 at the z=1.8" minimum the squared amplitude of the observed surface charge density is 50% greater than the corresponding value measured for smaller z. It should be noted that at this scan we are a distance of 1.7" (4.3cm) from the end of the hollow circular tube. Alternatively these scans are about 0.19λ from the ends. Thus the deviation in behaviour of the z=1.8" scans from those for smaller z can be predominantly attributed to the effects of ends of the finite length tube. These effects are further enhanced by taking scans of the squared amplitude of the surface charge density

further out along the axis. In figure 13 we show the measured results around the cylinder at z=2.7" (6.86cm). At this position along the cylinder axis the distance from the scanned circle to the nearby tube end is 0.8" (2.03cm) = 0.087λ. As we can readily observe in figure 13 the squared amplitude of the surface charge density starts out from the null at $\phi=0°$ on the side away from the source and monotonically increases to a maximum at about $\phi=\pm 34°$ as we move toward increasing ϕ values. The azimuth at which this maximum occurs is only slightly larger than that corresponding to smaller z values i.e. for scans further from the ends of the tube. At this maximum the amplitude has dropped slightly from the height observed for z=1.8 and is about that for the measured value for z=0.9". It should be emphasized however that the experimental values for the amplitudes in this region of ϕ are all pretty much the same. The differences amount to about 7-8%. With further increase in azimuth the z=2.7" scan is qualitatively the same as those for smaller values of z. We first note a continuous drop in the squared amplitude of surface charge density to a minimum at about the same azimuthal position as found for the other scans. Now however we note a further marked increase in height at the minimum. The height here is about 1/3 over that for the z=1.8" scan and about 50% above those for the z=0 and z=0.9" scans. Moving further around the tube we see that at z=2.7" the results indicate the same qualitative characteristics as those for smaller z. In the z=2.7" case however the amplitude squared is noticeably higher than was obtained for smaller z until

way around on the side facing the source. From $\phi \approx 132°$ on to $\phi = \pi$ this departure in amplitude fades away and indeed the height for z=2.7" even lies slightly lower than the height for z=0.9" over part of this range of azimuth. The second maximum for the z=2.7" scan lies at about $\phi = \pm 90$ in common with the location of the other scans. At this maximum the z=2.7" scan is about 25% higher than the z=0 and z=0.9" scan maxima and about 10% higher than the corresponding maximum in the z=1.8" scan. There is again an inflexion point which is somewhat more difficult to find at z=2.7". It occurs at about $\phi = \pm 126°$ quite close to that position for smaller z scans. We thus note that moving closer to the end of this cylinder results in higher maxima and also higher amplitudes at the minima. Even the inflection point seems to indicate higher surface charge density as we approach the tube ends. These changes occur while the locations of the maxima, minima and inflection points remain almost unchanged with location along the axis of the tube.

Figure 13 also displays super-imposed on the experimental results the theoretical squared amplitude of surface charge density for an infinite cylinder. The infinite cylinder has the same circumference to wavelength ratio $\gamma = \pi D/\lambda = 2.40$ and the normally incident radiation was assumed H-polarized. The theoretical distribution for the infinite cylinder as shown in figure 13 was normalized to the measured value at z=0 for $\phi = \pm 45°$. It is immediately evident that the infinite cylinder distribution displays the same characteristics as the measured scans. It predicts a null at $\phi = 0°$ followed by a

continuous rise to a maximum, then a continuous decrease to a minimum followed by a continuous increase to a second higher lying maximum. From this higher maximum it drops monotonically to zero at $\phi=\pi$ after first passing through a point of inflexion. Even though there is a strikingly close resemblance of the measured data for all positions of the scanning circle along the cylinder axis, to the normalized theoretical predictions for the induced surface charge density on the infinite cylinder there are some clear differences that standout in figure 13. First the squared amplitude for the infinite cylinder lies below all the measured distributions up to $\phi=\pm45°$, the fitting point for z=0. As ϕ increases from this azimuth to about $\phi=\pm65°$ the squared amplitude of the surface charge density on the infinite circular cylinder successively climbs above that measured for increasing distance from the center of the finite length cylinder. The first theoretical maximum occurs at $\phi=\pm35°$, just beyond the measured first maxima. The first minima which is just a shallow dip in the theoretical curve occurs at about $\phi=\pm52°$ which is somewhat sooner than observed for the scans on the finite length circular tube. From the first minimum on the theoretical curve continues to lie significantly higher than the measured scans for z=0 and 0.9" i.e. near the finite tube center line. For ϕ from $\pm55°$ to about $\pm90°$, the normalized theoretical predictions are about the same as the measured values for the scans taken closer to the tube ends. The second and higher maximum in the theoretical curve occurs at about $\phi=\pm95°$. This is located somewhat past the top and

bottom of the infinite cylinder towards the source and is about 5° further around than all the corresponding observed maxima. The theoretical inflection point is not too markedly visible but does occur at about the same azimuthal position as found for the scans of the finite length cylinder. From about $\phi=\pm 100°$ on around the infinite cylinder theory predicts that the squared amplitude of the surface charge density will exceed that for the finite length cylindrical tube. The difference is in fact quite large for azimuths from $\phi=\pm 115°$ to $\phi=\pm 145°$. All in all, however, inspection of figure 13 suggests rather strongly that the infinite cylinder induced surface charge distribution is a rather good approximation to the same quantity for the finite cylinder over most of its length. This is so provided we are not too close to the cylinder ends and if the length of the finite cylinder is about one-wavelength in size. It would thus appear that for such cylinders (recalling $\gamma=2.40$) one can use the predicted infinite cylinder surface charge distribution and one measurement for the finite cylinder at $z=0$ and say $\phi=\pm 45°$ and have the surface charge distribution for the entire finite length tube, except very near the ends. For most practical purposes this distribution would be satisfactory.

4. Surface Current Distribution on the Outside Wall of the Hollow Open Ended Circular Tube.

We can compare our measurements of the squared amplitude of each of the components of surface current on the outside wall of the open ended tube with two separate theoretical modes of solution.

The first is that of the asymptotic limit of an illuminated circular cylinder of infinite length. Comparison of empirical results with the theoretical predictions for the induced surface current distribution on an infinite cylinder enables us to determine how useful the relatively simple ideal solution is for describing the currents on a real, three dimensional, circular, open ended tube. In carrying out such comparisons limitations naturally present themselves to guide us in using the infinite cylinder as an approximate means of predicting the currents on a finite length, open, hollow, circular cylinder. The second theoretical mode of solution that of C. C. Kao[14-17] is in fact only an approximate attempt at analytic resolution for the diffraction characteristics of the finite length, empty, open, circular tube. Comparison with the measured results permits us to establish the degree of accuracy represented by that theory for the finite tube. Further, by detailed examination of both the measured data and the calculated currents for a finite tube, insight can be gained into the reasons for the shortcomings of the approximate theory.

Comparison of the data with predicted values of the currents from both the infinite cylinder theory and the finite tube theory for the two tubes measured thus give us quite valuable information for the general problem of diffraction by a finite, circular, open tube.

---

14. C. C. Kao, op. cit.
15. C. C. Kao, op. cit.
16. C. C. Kao, op. cit.
17. C. C. Kao, op. cit.

The first set of data to be discussed are those shown in figure 14. Included in this figure are circular scans around the tube at fixed distances along the cylindrical axis. These azimuthal scans are the measured values of the squared amplitude of the ϕ-component of magnetic field, just off the outer surface of the tube, per unit incident magnetic field amplitude squared. Except for a very small, and insignificant error, these scans are identical with the corresponding scans of the squared amplitude of the z-component of surface current on the outside wall of the finite length, open, tube at the same positions. Because of symmetry the results obtained for fixed z, are identical with the current component on the other side of center at -z. We exhibit explicitly the scans of $|K_z(\phi,a)|^2$ vs ϕ for z=o, i.e. in the plane perpendicular to the cylinder axis and bisecting the cylinder, and in parallel planes corresponding to $z = \lambda/4 = 0.21\ (L/2)$, $z = \lambda/2 \simeq 0.42\ (L/2)$, $z = 3\lambda/4 \simeq 0.63\ (L/2)$, $z = \lambda \simeq 0.84\ (L/2)$ and $z \lesssim L/2$. Juxtaposed on these measured data are calculated values for $|K_z(\phi,a)|^2/|H_o|^2$ for the infinite cylinder with circumference to wavelength ratio $\gamma \equiv \pi D/\lambda = 3.82$ and assuming the incident radiation is directed normal to its axis and is polarized parallel to that axis. At $\phi = 180°$ i.e. on the side facing the incident E-polarized incoming radiation the infinite cylinder prediction for the surface current has been normalized to the measured value for the finite tube at the point ϕ=180° and z=o. The finite tube also has been illuminated at broadside, normal incidence by plane radiation of wavelength λ=12.3cm polarized parallel to its

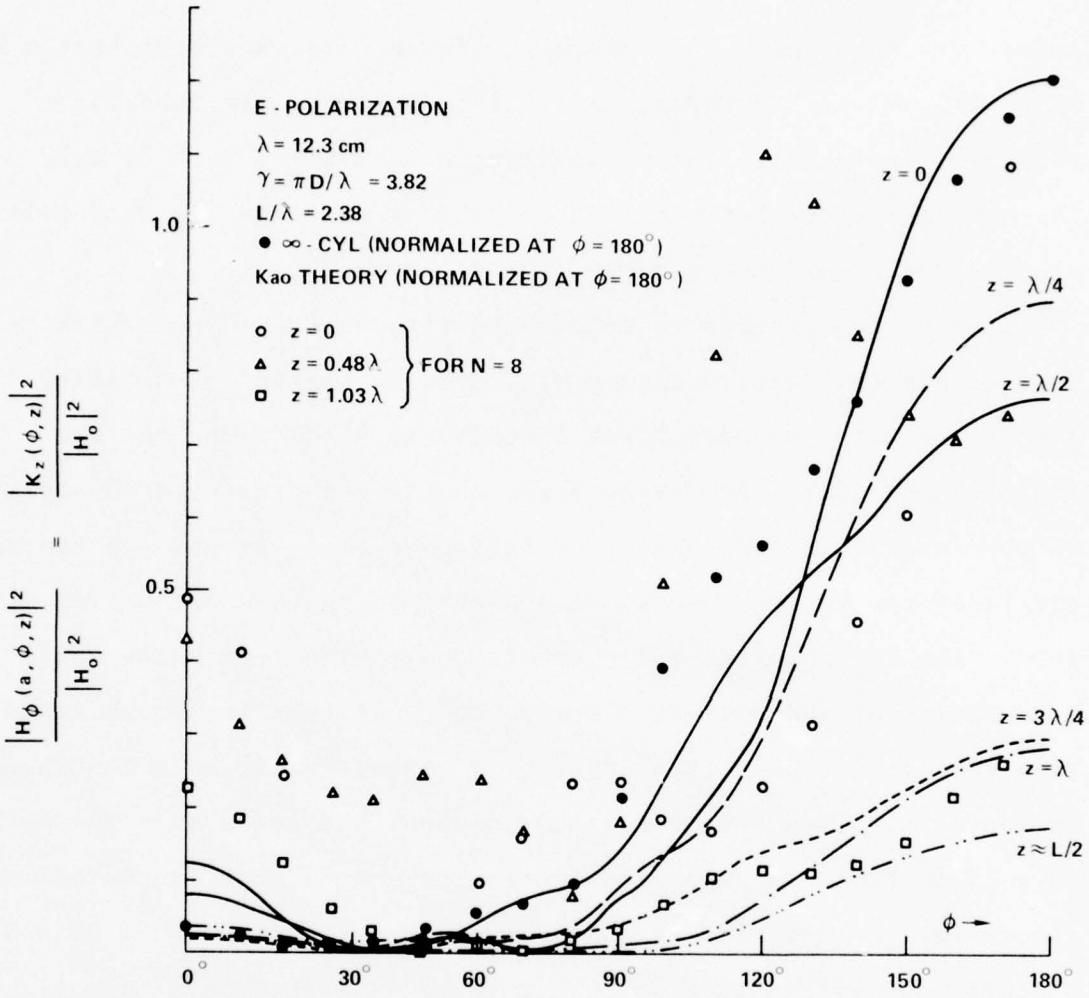

FIG.14 ANGULAR DISTRIBUTIONS OF SURFACE CURRENT $|K_z|$, ALONG A HOLLOW CYLINDRICAL TUBE OF DIAMETER D = 6 1/8" (15.6 cm) AND LENGTH L = 12" (30.5 cm).

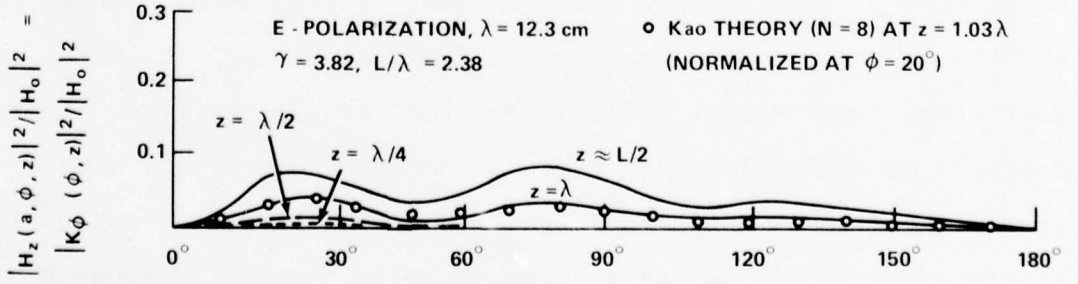

FIG.15 ANGULAR SCANS OF AZIMUTHAL SURFACE CURRENT ALONG OPEN ENDED HOLLOW CYLINDRICAL TUBE OF D = 15.6 cm, L = 30.5 cm.

axis. For the finite tube the circumference to wavelength ratio is also $\gamma=\pi D/\lambda=3.82$. However, the finite, hollow, open tube has a length to incident radiation wavelength $2h \equiv L/\lambda=2.38$. Clearly the best agreement between finite cylinder data and infinite cylinder predictions should occur around the z=0 scan.

Let us now proceed to a detailed discussion of the empirical surface current results accompanied by a corresponding detailed comparison with the normalized theoretical predictions for the infinite cylinder. Focussing first on the measured squared amplitude of the longitudinal component of surface current around the central circle of the finite tube we find a maximum on the shadow side at $\phi=0°$. The current then falls continuously with increasing angle ϕ to vanish at the null at about $\phi=\pm 36°$. It then increases steadily to a second but lower lying maximum at about $\phi=\pm 54°$ as ϕ continues to increase. This second maximum is about 80% lower than the peak at $\phi=0°$ on the side away from the source. Note that the normalized theory for the infinite cylinder also shows a maximum at $\phi=0°$ and a continuous attenuation with increasing azimuth ϕ until a null appears at about the angular locations as measured on the finite length tube. The infinite cylinder peak at $\phi=0°$ is only about 25% as high as the measured maximum for the finite length cylinder. Unlike the experimental observations the infinite cylinder theory predicts an increasing longitudinal component of current with increasing azimuth until the angular position $\phi \approx \pm 76°$ at which it displays not a maximum but a point of inflection. The squared

current at this inflection point is about 100% higher in amplitude than that at $\phi=0°$. However the measured amplitude squared for the longitudinal component of current and the theoretically predicted value (normalized at $\phi=180°$) for the infinite cylinder are comparable at the azimuth for the second measured peak of the z=0 scan. We observe that as ϕ increases beyond that for the second peak in the measurements the observed amplitude again falls off steadily to a very small amplitude, almost vanishing, at $\phi\approx\pm71°$. This just precedes the first inflection point in the infinite cylinder prediction for the corresponding surface current amplitude. Following this very low lying observed minimum the experimental data show a quick rise with increased azimuthal angle to a point of inflection at about $\phi=\pm89°$. Thereafter the measurements display some barely discernible structure for the next few degrees as ϕ increases over the top around to the illuminated side accompanied by an increase in amplitude. Once on the side of the finite tube facing the incoming plane wave the squared amplitude of the longitudinal current increases steadily and quite sharply with increasing ϕ until another inflection point is observed in the empirical results at about $\phi\approx\pm116°$. The infinite cylinder predicts on the other hand a similar behaviour from the inflection point at $\phi\approx\pm76°$ to a subsequent inflection point at about $\phi\approx\pm125°$. Between the two inflection points on the theoretical curve for the current on the infinite cylinder the predicted amplitude for the longitudinal current component lies considerably higher than was observed, over

the same range of azimuthal variable, for the measured component for the finite length, open-ended tube. It is quite clear from even a casual glance at figure 14 that the infinite cylinder theory quantitatively deviates markedly from the observations for the finite cylinder for this range of azimuth. It is nevertheless interesting to note that, qualitatively, they are similar over this range of ϕ. From $\phi = \pm 125°$ the measured distribution rapidly rises with further increase in ϕ to its highest value at $\phi=180°$ which is an order of magnitude larger in value than the measured peak on the very back of the finite tube at $\phi=0°$. The normalized infinite cylinder prediction for $|K_z(\phi)|^2$ over this range of ϕ exhibits much the same behaviour as the measured squared amplitude of $|K_z(\phi,a)|^2$ for the finite cylinder. Summing up we note that the infinite cylinder theory, assuming normalization to the measured value for $|K_z|^2$ at $\phi=0°$ in the $z=0$ plane, closely approximates the empirical current amplitude for the finite length circular tube from $\phi \approx \pm 130°$ to $\phi=180°$. The agreement is rather poor over the range from $\phi \approx \pm 80°$ to $\phi \approx \pm 130°$. For the remainder of the azimuthal scan they again are in more or less good agreement. Utilizing C. C. Kao's computer program in its highest order of approximation, which gave its best theoretical results, we calculated his prediction for the azimuthal distribution for the squared amplitude of the longitudinal current component for the same scattering problem studied in the laboratory. The distributions obtained for different z values from the Kao theory for the finite open ended tube are also depicted in

figure 14 simultaneously with the infinite cylinder theory predictions and the measured current scans. We also normalized the numerical results obtained from Kao's theory to the measured results at $\phi=180°$. Consider the normalized distribution for $|K_z(\phi,a)|^2$ as given by Kao's theory around the central scan. At $\phi=0°$ Kao predicts a maximum which monotonically decreases as ϕ increases until it predicts a null at about $\phi \approx \pm 37°$ which lies quite close to the position of the measured null. Although we observe a rather good qualitative agreement of the theoretical prediction for the longitudinal current components amplitude with the measured results over this range of azimuth the same situation does not hold quantitatively. The peak predicted by Kao at $\phi=0°$ is about 4 times higher than the measured value. Over the range of ϕ from 0° to the first null at $\phi \approx \pm 37°$ the Kao prediction for the current is quantitatively far apart from that predicted for the infinite cylinder. With further increase in azimuth the Kao prediction for $|K_z(\phi,a)|^2$ shows a steady increase to a second lower peak at about $\phi \approx \pm 85°$. This disagrees both qualitatively and quantitatively with the measurements and also the current predicted by infinite cylinder theory. Kao's theory then indicates that the longitudinal current component amplitude decreases with increasing azimuth until another high lying minimum appears at about $\phi \approx \pm 113°$. It should be noted that this minimum in the Kao theory for the longitudinal component of current lies in the vicinity of inflection points found in the experimentally obtained scan and also in the infinite cylinder

predictions. From $\phi \approx \pm 120°$ on to $\phi = 180°$ Kao, the infinite cylinder and the measurements all exhibit qualitatively the same rapid rise to a high maximum at $\phi = 180°$. However the Kao current over this range lies considerably lower than the experimentally obtained current and the normalized infinite cylinder prediction for $|K_z|^2$. Of course all three coincide at $\phi = 180°$. At this point we can make the observation that the Kao theory for $z=0$ appears to be of questionable reliability for predicting $|K_z(\phi,a)|$ for a finite tube.

Next we examine the distribution of the squared amplitude of the longitudinal component of current around the finite length tube at $z=\lambda/4$ i.e. about one-fifth of the way from the central scan toward the open end. Only the experimentally obtained scan is shown in figure 14 for $z=\lambda/4$. It should be recalled however that the infinite cylinder limit predicts a longitudinal component of current that is the same for all values of z along the cylinder. Thus we can compare our measured data with the same normalized infinite cylinder predictions for the value of $|K_z(\phi,a)|^2$ shown in figure 14. A casual glance at the two sets of results for $z=\lambda/4$ reveals qualitative similarities between them. They both have a low lying peak at $\phi = 0°$ with the experimental value lying at about half the height of the infinite cylinder value there. The measured data show a steady decrease to a minimum at about $\phi = \pm 32°$. At this minimum the height is about half that of the peak at $\phi = 0°$. Note that this minimum occurs somewhat before the null in the infinite cylinder distribution at $\phi \approx \pm 36°$ which by the way is the

locale at which the z=0 null also occurs. Note also that the $z=\lambda/4$ peak at $\phi=0°$ is about one-fifth as high as that for the z=0 distribution. Continuing the $z=\lambda/4$ scan on around the cylinder we find that the measured amplitude of the longitudinal component of surface current steadily increases to a second low lying maximum at about $\phi=\pm 53°$. This peak is very close to the one observed on the z=0 scan of longitudinal surface current and furthermore both rise to about the same height. Unlike the z=0 surface current scan the second peak for the $z=\lambda/4$ current distribution is just under twice that of the $\phi=0°$ peak. With further increase in the azimuthal variable we observe a non-vanishing second minimum in $|K_z(\phi,a)|^2$ for $z=\lambda/4$ at about the same value of ϕ for the $\phi=0°$ scan. Unfortunately some rather indistinct structure in the measured amplitude of surface current for $z=\lambda/4$ in this neighborhood of ϕ blurs the actual detailed behaviour. Just as observed earlier in the z=0 scan we note that the measurements for $z=\lambda/4$ reveal a point of inflection just before ϕ reaches the top of the tube at 90°. With further increase in the azimuthal variable so that we are around on the side facing the source we find just as for the infinite cylinder and the z=0 scan of $|K_z|$ the amplitude rises and passes through another inflection point on the $z=\lambda/4$ scan. For the latter this point appears earliest at about $\phi=\pm 102°$. From there on around the amplitude of the longitudinal current component squared for $z=\lambda/4$ behaves just as the corresponding quantity for z=0 in that it rises monotonically to its highest value, a maximum, at $\phi=180°$.

Here at $\phi=180°$ the height of the peak for $z=\lambda/4$ is about three fourths that for $z=0$. It is also worth noting that from $\phi=\pm30°$ to about $\phi=\pm120°$ the amplitudes measured for $z=0$ and $z=\lambda/4$ are pretty nearly the same with both lying substantially lower than the infinite cylinder theory predicts. Next we consider the azimuthal scan of $|K_z(\phi,a)|^2$ at $z=\lambda/2$ as found experimentally and the corresponding normalized prediction of that quantity calculated via Kao's computer program. Actually we calculated with Kao's technique at $z=0.48\lambda$. The difference from the distribution at exactly $z=\lambda/2$ should be quite insignificant. At half a wavelength from the centerline scan we find the expected peak at $\phi=0°$. This maximum has a height about halfway between that for $z=0$ and that for $z=\lambda/4$. As the azimuth increases the measured squared surface current amplitude continuously drops until it vanishes at about $\phi=\pm43°$. Note this minimum occurs at a somewhat larger value of ϕ than we observed in the measurements earlier for smaller z, as well as the azimuth predicted by infinite cylinder theory. Kao's theory does predict a minimum in this neighborhood of ϕ but it yields a relatively high lying and non-vanishing amplitude. His normalized theory also predicts a maximum for $\phi=0°$ with height comparable to that for $\phi=0°$ and $z=0$. The Kao peak at $\phi=0°$ for $z=0.48\lambda$ is about five times as high as the measured value there. The $z=\lambda/2$ measured distribution for $|K_z(\phi,a)|^2$ rather closely follows the infinite cylinder theory from $\phi\approx\pm45°$ up to about $\phi\approx81°$. Beyond $\phi\approx55°$ we find the measured distribution at $z=\lambda/2$ lies above the distributions

for smaller z but below the infinite cylinder predictions up to about $\phi \approx 120°$. It still displays about the same qualitative characteristics as the infinite cylinder theory predicts although it lies substantially lower all the rest of the way around to $\phi=180°$. The $z=\lambda/2$ scan resembles the $z=\lambda/4$ scan lying above it from about $\phi \approx \pm 60°$ crossing it at $\phi \approx \pm 136°$ and then lying above it the rest of the way and also reaching a maximum at $\phi=180°$. At this point we are beginning to discern an evolution in the measured angular distribution of $|K_z(\phi)|^2$ for the finite length tube as z increases from the central value. This evolution in behaviour is the direct consequence of the finite length of the tube. It is quite significant to note the angular distribution predicted by the Kao theory for $|K_z(\phi,a)|^2$ at $z=0.48\lambda$. We have already observed that this theory yields a high lying peak at $\phi=0°$ followed by a high lying minimum. It then predicts a small rise to a second maximum at about $\phi \approx \pm 54°$. This is not too surprising. However what follows this as ϕ increases is quite interesting. We find another relatively low-lying minimum at about $\phi \approx \pm 80°$ and then a remarkably steep ascent to a very high peak at about $\phi \approx \pm 120°$ another steep drop to a minimum near $\phi \approx \pm 160°$. The height of this minimum is almost equal to that of the maximum for $\phi=180°$ and $z=\lambda/2$. In turn the Kao theory then predicts a small increase with ϕ to a peak at $\phi=180°$. The predicted behaviour of this current distribution at $z \approx \lambda/2$ obtained from the Kao theory is very radically different qualitatively and quantitatively from the experimental observations for the finite length tube and also

the limiting case of the infinite cylinder. This departure is so significant as to raise serious questions concerning the reliability of the Kao analytic solution. Reinforcement of these doubts is added by considerations we shall make later concerning the other component of surface current - namely this component, $|K_\phi|$, is quite small at $z \approx \lambda/2$ as was found both experimentally and by Kao's theory. Note, in passing, for $z \approx \lambda/2$ we are about half way between the center of the finite tube and its end. Now let us move further out along the hollow, open ended circular tube to $z=3\lambda/4=0.63\left(\frac{L}{2}\right)$. We are now scanning on circles closer to the tube end than to the tube center. Not unexpectedly we find from here on out along the z=axis that $|K_z|$ decreases quite rapidly overall as the end of the tube is approached. Note K_z is directed normal to the tube edges. Experiment again shows a maximum at $\phi=0°$. This peak has a height about equal to that for the peak observed at $\phi=0°$ and $z=\lambda/4$. With increasing ϕ the measured squared amplitude $|K_z(\phi,a)|^2$ falls off, lying just below the corresponding quantity for $z=\lambda/4$, to vanish at a minimum at about $\phi \approx \pm 36°$. With further increase in the azimuthal variable ϕ the measurements reveal an increasing $|K_z(\phi,a)|^2$ which almost coincides with the measured results for the $z=\lambda/4$ scan until about the value of azimuth $\phi \approx 80°$. We observe by inspection of figure 14 that from $\phi \approx 60°$ to $\phi=180°$ the empirically obtained distribution at $z=3\lambda/4$, $|K_z(\phi,a)|^2$, is quite similar qualitatively to the measurements obtained at $z=\lambda/2$ over that range of azimuth. Both of these experimental distributions are qualitatively very much

like that predicted for the infinite cylinder over the same range of angle ϕ. The principal difference exhibited by the measured results for the longitudinal surface current distribution at $z=3\lambda/4$ is manifested by the high degree of attenuation of the amplitude. For purposes of illustration we note that the maximum peak height at $\phi=180°$ and $z=3\lambda/4$ is about half that measured at $\phi=180°$ and $z=\lambda/2$ and is also about one fourth that for $\phi=180°$ and $z=0$.

Continuing out to the angular distribution of $|K_z(\phi,a)|^2$ obtained at $z=\lambda$ we again can compare experimental results with infinite cylinder theory and with calculations from Kao's theory. Although the latter surface current was determined for $z=1.03\lambda$ it should be very close to the surface current distribution for $z=\lambda$ itself. The measurements of $|K_z(\phi,a)|^2$ for $z=\lambda$ show that the amplitude of this component of current is very small up to about the azimuthal angle $\phi \approx \pm 60°$. Nevertheless it still shows the same structural characteristics for lower ϕ values as observed for smaller values of z. This behaviour we shall see reflected in the measurements for $|K_\phi(\phi,a)|^2$ at $z=\lambda$. For larger values of azimuthal angle we note a very slow variation in the squared amplitude of the longitudinal surface current component. This rate of change is so slow that it drastically masks the structural detail of the surface current distribution until ϕ attains the value $\approx \pm 100°$. At that point a barely discernible point of inflection can be found in the experimental data. Thereafter as

ϕ increases $|K_z(\phi,a)|^2$ at $z=\lambda/2$ increases to a peak at $\phi=180°$. The height of this peak is quite low lying just under the corresponding value for $z=3\lambda/4$. We again see in the measurements a rapid attenuation, around the tube, of the component of surface current directed normal to the tube end as that end is approached. Although there are still vestiges resembling the qualitative behaviour of the infinite cylinder theory predictions we are sufficiently close to the tube end to have radical departure from that theory clearly evident. Consider now the prediction for the angular distribution of $|K_z(\phi,a)|^2$ obtained from the Kao theory at $z\approx\lambda$ normalized, of course, to the experimental value at $\phi=180°$. We observe first of all in figure 14 that this theory does reflect the necessary physical requirement that on the average around the tube the longitudinal surface current amplitude must decrease as the tube end is approached. Clearly it lies well below the $z\approx\lambda/2$ surface current distribution. The Kao theory exhibits clearly some well defined structure on the back side of the tube. We see a peak at $\phi=0°$ followed by a steady drop off to a minimum or null at about $\phi\approx\pm50°$ and then a small rise to a very low lying maximum at about $\phi\approx\pm60°$ a subsequent drop to another null at about $\phi\approx\pm70°$ and then a gradual rise in amplitude with increasing azimuth ϕ. This increase continues with increasing ϕ until around on the front side of the tube we are able to make out the occurrence of another maximum at about $\phi\approx\pm120°$. The appearance of this maximum in Kao's theory for the finite tube once again implies

that there are some questions as to the reliability of the solution. As ϕ increases further we observe the passage through another minimum in $|K_z(\phi,a)|^2$ at $\phi \approx \pm 133°$ for Kao's theory at $z \approx \lambda$ and then a rapid rise to the peak at $\phi=180°$. Note that the normalized curve from the Kao theory predicts the surface current amplitude near $\phi=0°$ to be about an order of magnitude higher than experiment shows for $z \gtrsim 3\lambda/4$. The final set of measurements for the angular distribution of $|K_z(\phi,a)|^2$ was made very close to the end of the finite, hollow, open tube. What we observe is a maximum at $\phi=0°$ lying slightly above those for $z=\lambda/4$ and $z>3\lambda/4$. As ϕ increases the surface current amplitude for K_z at $z \approx L/2$ remains quite small and displays some structure including a null at about $\phi \approx \pm 75°$. This is followed by a very slow rise as ϕ increases up to about $\phi \approx \pm 122°$ well around on the front side facing the incoming radiation. At this point an inflection point appears. $|K_z(\phi,a)|$ then continues to increase as ϕ increases until it attains its maximum at $\phi=180°$. Note that at $\phi=180°$ the peak height in figure 14 for $z \approx L/2$ is only about one-half that at $z=3\lambda/4$ or $z=\lambda$ and lies well below that for smaller values of z. Again we observe a further attenuation in $|K_z(\phi)|$ as we approach the tube end. Near the end of the tube we find $|K_z(\phi,a)|^2$ is quite different from the infinite cylinder theory although some resemblances do persist.

In summary we note several general characteristics. Normalizing Kao's theoretical distributions to the experimental values at $\phi=180°$ results in significant quantitative disagreement on the shadow side

near $\phi=0°$. This is not the case when the infinite cylinder theory is so normalized so long as we do not get too close to the ends. Qualitatively there is considerable similarity between the experimentally obtained surface current distributions and that predicted by infinite cylinder theory. On the other hand the Kao theory does predict some serious disagreement with both infinite cylinder theory and measurements as well.

In order to complete the picture for the surface current distribution on the finite, hollow, open, circular tube we must consider the remaining component of surface current namely the azimuthal component K_ϕ. For the limiting case of the infinite cylinder this component does not exist at normal incidence. The sets of measured distributions for $|K_\phi(\phi,a)|^2$ along the finite cylinder and the calculated currents from Kao's theory are shown in figure 15. At $z=0$ we obtained identically zero amplitudes for the measured results for all ϕ for K_ϕ which is consistent with the symmetry requirements for the surface current components over the finite open circular tube. The Kao theory coincides with the measurements at $z=0$. For $z=\lambda/4$ the squared amplitude of $|K_\phi(\phi)|^2$ was measured and found to be too small to include in figure 15. We should note that all of figure 15 would fall at the very bottom portion of figure 14, i.e. $|K_\phi|$ except possibly at the very edge of the finite circular tube is very small for all values of azimuth ϕ. At $z=\lambda/2$ we find the measured distribution has achieved amplitudes that are significant enough to include in figure 15. What

hollow circular cylindrical tube. The magnetic field of the incident

we observe are a null at $\phi=0$ where K_z has a maximum a slowly increasing amplitude as ϕ increases -- opposite to the behaviour displayed by K_z -- to a very low-lying peak at about $\phi = \pm 33°$. This is about where the corresponding $|K_z|$ has a minimum. $|K_\phi|$ then decreases with increasing ϕ to a null at about $\phi=\pm 50°$ and remains very small thereafter as ϕ goes to 180°. Note that roughly speaking $|K_z|$ is larger for the side facing the source than for the side facing away from the source. $|K_\phi|$ on the other hand exhibits exactly the opposite behaviour. Nevertheless for $z \lesssim \lambda/2$ $|K_\phi|$ is quite small. The angular distribution measured for $z=\lambda$ is very much the same as that for $z=\lambda/2$. It would appear that the principal difference is that for $z=\lambda$ the amplitude is somewhat larger over the angular scan. We note that for $z=\lambda$ $|K_\phi(\phi,a)|^2$ has a second maximum at about $\phi \approx \pm 80°$. This peak is slightly lower in height than the first one. Further increase in azimuth reveals some slight structure in $|K_\phi|^2$ and a slow relatively smooth drop off to zero at $\phi=180°$ where $|K_z|^2$ has its maximum value. We have superimposed on the measured $|K_\phi|^2$ distribution at $z=\lambda$ the Kao theory's predictions normalized to agree with experiment at $\phi=20°$ but for $z=1.03\lambda$. These are pretty close to the theoretical values for precisely $z=\lambda$. The results indicate very close agreement with the measured distribution for $|K_\phi(\phi,a)|^2$. It should however be kept in mind that this surface current component is indeed quite small. We next note that for the scan around the finite open, circular tube in toward the center at $z=3\lambda/4$ we find the empirical results

indicate a marked drop in amplitude below that observed at $z=\lambda/2$. Finally we consider the measured surface current distribution of $|K_\phi(\phi,a)|^2$ for $z\approx L/2$ i.e. out close to the end of the finite length tube. The first observation we can make from a glance at figure 15 is that out here the current $|K_\phi(\phi)|$ is the largest. Roughly speaking the amplitude for $z\approx L/2$ is about twice that for $z\approx\lambda$ and about an order of magnitude higher than for $z\approx\lambda/2$. For $z\approx L/2$ not only is the same qualitative character seen that was found for smaller z for $\phi\lesssim 100°$ but we can make out some additional structural features namely another maximum at about $\phi\approx\pm 130°$ and then a decrease with increasing azimuth around to $\phi=180°$. We also note a qualitative difference from $|K_\phi|^2$ for smaller z. This is the higher peak occurs at $\phi\approx\pm 75°$ just around on the backside rather than near $\phi\approx\pm 25°$. Briefly summarizing what we have found for $|K_\phi(\phi,a)|^2$, we note that its behaviour is roughly complementary to that of $|K_z(\phi,a)|^2$ i.e. maximum and minima interchange. Also $|K_\phi|^2$ is quite small and very likely only becomes appreciable as we get very close to the ends of the finite, open tube.

As we have seen the Kao analytic solution for the finite, circular, open ended, hollow tube appears to be somewhat unsatisfactory. This is certainly true for cylinder lengths that exceed the wavelength of the incident radiation. It would then appear that investigations of a hollow, open circular cylinder with length to wavelength ratio, $2h/\lambda = L/\lambda < 1$ should be more appropriate for testing the Kao analytic results. Since our second cylinder has a

length to wavelength ratio $L/\lambda = 0.766$ the results of the corresponding measurement program provide a vehicle for effecting this evaluation of Kao's theoretical predictions. Of course the empirical results themselves independently provide us with an important set of data that characterize a finite, hollow, open circular tube.

The next cylinder subjected to experimental investigation was of diameter D=7"(17.78cm) and length L = 7". For this cylinder the wavelength of the normal, broadside incident radiation was $\lambda = 23.2$cm. Thus for these studies the essential parameters of the problem were: (1) the ratio of circumference to incident wavelength, $\gamma = \pi D/\lambda = 2.40$ and (2) the ratio of cylinder length to incident wavelength, $2h/\lambda = L/\lambda = 0.766$. What we have is indeed a short, fat tube in this case. However the dimensions are not asymptotic in any sense. Not only can we assess the relability of the Kao theory for this cylinder but we can also evaluate the extent to which infinite cylinder theory can be safely used to predict surface currents for this short tube. Although it would at first seem somewhat far fetched to utilize infinite cylinder theory for such a short cylinder we shall see below that this approach has its merits.

The first case investigated for this cylinder was for the incident radiation polarized parallel to the axis of the tube. This is the E-polarization case. Scans of the angular distribution of the squared amplitude of each of the components of surface current were made around circles in planes through the center of the cylinder,

length circular cylindrical tube. It also contains the corresponding

i.e. at $z = 0$, and in planes displaced from the center at $z = L/8 = 0.096\lambda$, $z = L/4 = 0.192\lambda$, $z = 3L/8 = 0.288\lambda$, and out near the ends of the tube at $z \lesssim L/2 \approx 0.38\lambda$. Observation of the data revealed just as for the longer cylinder studied earlier that in each case $|K_j(\phi,z)| = |K_j(\phi,-z)|$ and $|K_j(\phi,z)| = |K_j(-\phi,z)|$. Consequently we once again need only to present here the results for $0 \leq \phi \leq 180°$ and $0 \leq z \leq L/2$.

Let us begin the discussion by considering the infinite cylinder prediction for the surface current on a circular cylinder with $\gamma = 2.40$. For a normally incident E-polarized wave infinite cylinder theory predicts the existence of only an axial or longitudinal component of current on the outer surface. This current is independent of the z-coordinate. For the infinite cylinder at $\gamma = 2.40$ we have $K_\phi(\phi,a) \equiv 0$ for all ϕ and all z for the case of E-polarization. On the infinite cylinder we find a maximum at $\phi = 0$ for $|K_z|$. As the azimuthal variable increases this current drops to a minimum at about $\phi = \pm 30°$. With further increase in ϕ the amplitude of this surface current increases steadily passing through a point of inflection at about $\phi = \pm 100°$. It continues to increase with ϕ and attains a maximum at $\phi = 180°$. For the infinite cylinder the squared amplitude of K_z at $\phi = 180°$ is about 65 times that at $\phi = 0°$. For future reference it is also significant to note that the squared amplitude at $\phi = 0°$ is about 5 times that at the minimum in the vicinity of $\phi = \pm 30°$.

Let us next proceed to examine the experimentally obtained surface current distribution on the short, open tube for E-polarization of

the incident radiation. The empirical results obtained for $|K_z(\phi,a)|^2$ are shown in figure 16. Also included in figure 16 are the corresponding theoretical values for the infinite cylinder subjected to the same illumination. The infinite cylinder predictions have been normalized to the measured value at $z = 0$ and $\phi = 180°$. At $z = 0$ we first note that $|K_\phi(\phi)|^2 \equiv 0$ for all ϕ. Here we would naturally expect $K_z(\phi)$ to exhibit the closest approximation to the infinite cylinder characteristics. Inspection of the empirical angular distribution obtained for this component of surface current, as shown in figure 16, reveals that the qualitative character at $z = 0$ is nearly identical with that of the infinite cylinder. We find a maximum at $\phi = 0°$ followed by a minimum then an inflection point subsequently is clearly evident and finally a high maximum occurs at $\phi = 180°$. Although we have remarkable qualitative agreement of the finite cylinder measured distribution of $|K_z(\phi)|$ with the calculated infinite cylinder distribution we nevertheless have sharp differences in the quantitative characteristics of $|K_z(\phi,a)|$ for the finite and infinite cylinders. This is not too surprising since the length of the finite tube is only about three-fourths of the incident wavelength. At $z = 0$ we find the measured minimum at about $\phi = \pm 45°$ somewhat closer to the source than for the infinite cylinder. The inflection point in the measured distribution occurs at about $\phi = \pm 130°$ also shifted toward the source relative to the calculated infinite cylinder location of this point. For the measured current $|K_z|^2$ at the maximum at $\phi = 180°$ is only about four

peaks $\phi = 180°$ and $\phi = 0°$ is about five to one. At $\phi = 180°$ the

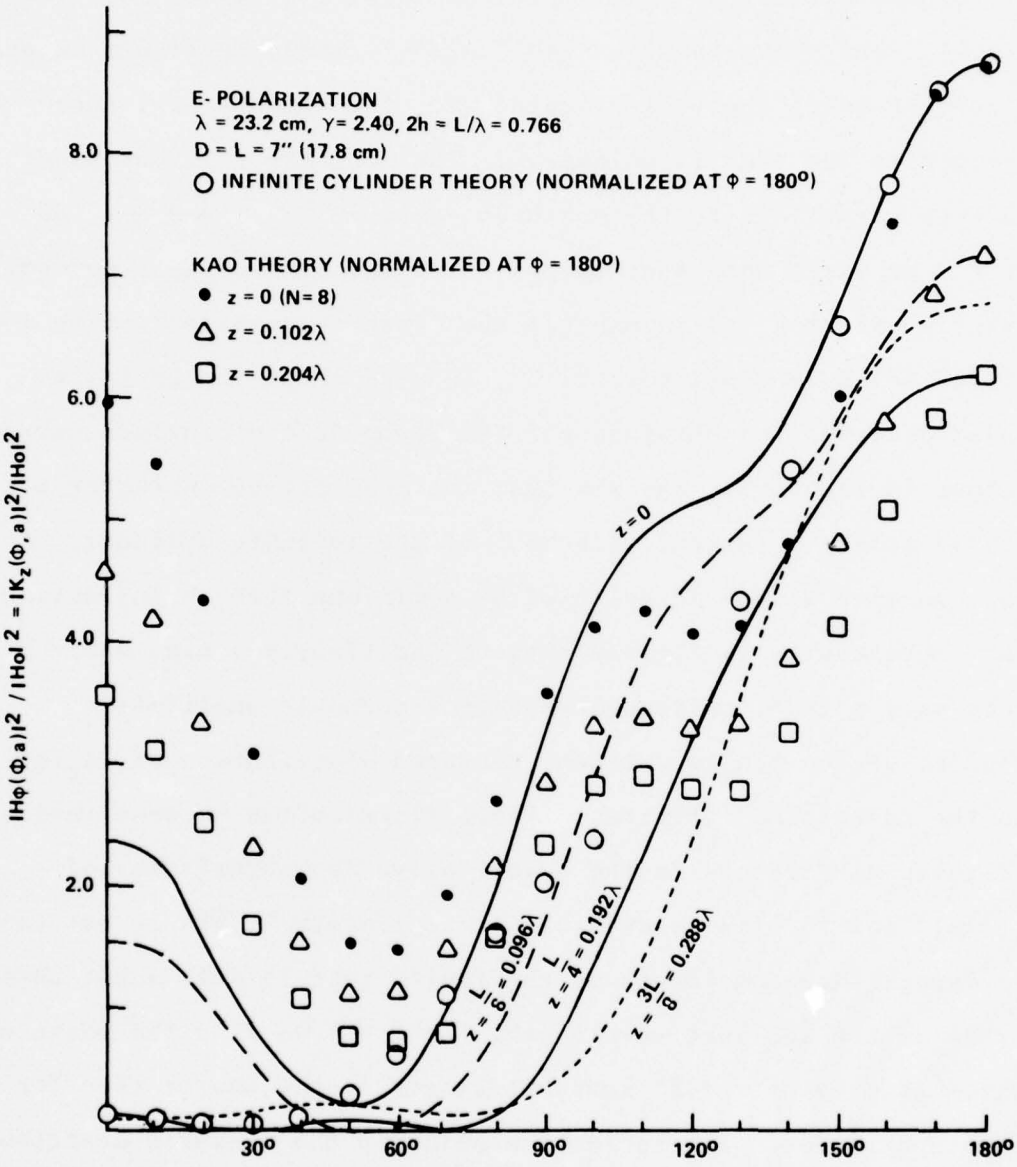

FIG. 16 ANGULAR DISTRIBUTION OF SURFACE CURRENT $|K_z|^2$ ALONG HOLLOW TUBE OF DIAMETER D = 7" (17.8cm) = LENGTH L FOR E-POLARIZATION

than about 107° the measured $|K_z|^2$ at worst lies below the measured

times that at $\phi = 0°$. This is about 1/16 the corresponding ratio for the infinite cylinder. Further the measured maximum of $|K_z|^2$ for the empty finite length tube at $\phi = 0°$ is about twelve times the value at the minimum of $|K_z|^2$ at $\phi \approx 45°$. This is about twice the corresponding theoretical ratio for the infinite cylinder. We thus observe at z=0 the first indications of the marked shifting of the infinite cylinder distribution necessary for obtaining the surface current on a finite length conducting tube whose length is less than the wavelength of the incident radiation. Very roughly speaking then we see from figure 16 that the normalized infinite cylinder distribution of $|K_z(\phi,a)|^2$ for many applications will probably be an adequate description of this current around the center of the finite tube. This is a reasonable approximation from the direction toward the source i.e. $\phi = 180°$ to the vicinity of the minimum at about $\phi = \pm 45°$. At $z = L/8 = 0.096\lambda$ we observe that the measured distribution of $|K_z(\phi,a)|^2$ is almost a duplication of that at $z = 0°$. The essential difference as we expect is a reduction in the amplitude at $z = L/8$. Since this scan represents a shift away from center of only about 1/10 of a wavelength and is still around a circle relatively well removed from the tube ends this is a quite reasonable result. As we move further down the open empty conducting tube towards the ends we observe strong qualitative changes in the measured angular distributions of the squared amplitude of the longitudinal component of surface current, $|K_z(\phi,a|^2$. Thus at $z = L/4 = 0.192\lambda$ we observe a general attenuation in the amplitude of this component of surface current all around the tube.

A minimum was observed at this outermost scan that lies at about

This attenuation is highly accentuated for $\phi < 45°$. Accompanying this behaviour we note that the inflection point near $\phi = \pm 130°$ is now imperceptible. Furthermore, the minimum for smaller z in the vicinity of $\phi = \pm 45°$ has now become a maximum although it has a rather small amplitude. This maximum has a minimum on either side of it at about $\phi = \pm 35°$ and $\phi = \pm 75°$. It should be pointed out that this low lying structure is in a region of quite low signal to noise ratio. Nevertheless we find that as we get even closer to the tube end at $z = 3L/8 = 0.288\lambda$ this behaviour on the side away from the source is again observed. This occurs at higher values of amplitude at this value of z. It would appear then from the experimental results that as we approach the ends the longitudinal current amplitude fluctuates. That is we observe a decrease as z increases until near the tube end where a slight increase occurs and then a very rapid drop is shown by $|K_z(\phi,a)|^2$ very close to the end of the tube. In fact the value of $|K_z(\phi,a)|^2$ is lost in the noise for $z \approx L/2$. In figure 16 we also included the results obtained using Kao's computer program at the limit of its accuracy. In each case the Kao results have been normalized to $\phi = 180°$ for the specified z-value. The normalized Kao distributions we note from figure 16 all have a maximum at $\phi = 0$ and another higher one at $\phi = 180°$. Instead of an inflection point they exhibit instead a minimum in the vicinity of $\phi = \pm 125°$ and of course an accompanying slightly higher maximum just before that at about $\phi = \pm 110°$. We note that this new maximum is about equal in amplitude to that at $\phi = 0°$ and is

about one-half that at $\phi = 180°$. Kao's theory predicts a deep minimum at about $\phi = \pm 55°$. At the minimum the Kao amplitude is about one-fourth that of the maximum at $\phi = 0°$. Note that for the larger values of z that is as we get closer to the tube end the values predicted by Kao for $|K_z(\phi,a)|^2$ remain rather flat for an extended range in the vicinity of the minimum. Unlike the measured distributions and the infinite cylinder predictions Kao's program implies on the average a much flatter distribution of current around the thick cylinder. On the side away from the source the normalized theory predicts currents that are much too high in amplitude. We point out that the values of z at which Kao's distributions were obtained were constrained by the requirements of his program. Nevertheless they can be normalized to closeby values of z at which the measured scans were made and this can be effected with negligible resulting discrepancies. On the whole it would appear that for the shorter cylinder the Kao theoretical results for $|K_z(\phi,a)|$ are in better agreement with the measured results and infinite cylinder theory. However they are still short of satisfactorily describing this current even for the case of $I/\lambda \approx 3/4$. This is the situation for E-polarization at any rate.

Next let us consider the distribution of the azimuthal component of current $|K_\phi(\phi,a)|^2$ over the open hollow conducting tube. As is well known $K_\phi(\phi,a) \equiv 0$ everywhere on the outer surface of an infinite cylinder for E-polarized illumination at normal incidence. A finite length tube similarly irradiated does have an angular component of

surface current. In principle this component is identically zero around the center of the finite tube. This was borne out very clearly by experiment. The Kao theory was formulated "a priori" to meet this requirement. According to conventional theory the angular component of current at the end of the finite tube becomes infinite in amplitude. Accordingly the Kao theory has been formulated to yield this result. In the laboratory of course this does not occur for a number of well established reasons. What does occur in reality is merely a growth in amplitude as the end of the tube is approached. Figure 17 shows the results obtained for the measured angular distributions of the squared amplitude of the angular component of surface current at various distances from the central circle. We see at $z = L/8$ a fairly uniform small angular component of current exists around the cylinder. This measured current is extremely small at $\phi = 0°$. It then rises slightly exhibiting traces of structural detail as ϕ increases and then drops to a minimum at $\phi = 180°$. At $z = L/4 = 0.192\lambda$ we see the measured results indicate a small current at $\phi = 0°$ which increases slightly to a maximum at about $\phi = \pm 30°$. It then steadily falls to a minimum at about $\phi = \pm 75°$. With further increase in ϕ we find another increase to a second maximum at about $\phi = \pm 120°$. At this second maximum the height is only about half that measured at the first maximum. As the azimuthal position moves further around toward the source $|K_\phi|^2$ drops monotonically to a minimum at $\phi = 180°$. Also shown in figure 17 is the Kao prediction for $|K_\phi(\phi,a)|^2$ at $z = 0.204\lambda$.

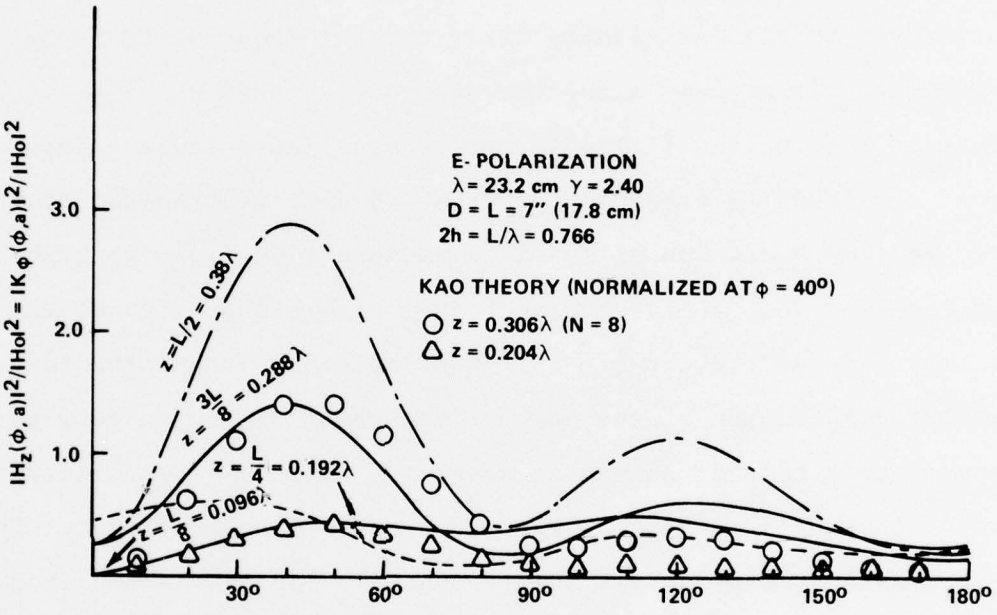

FIG. 17 ANGULAR DISTRIBUTION OF AZIMUTHAL COMPONENT OF SURFACE CURRENT $|K_\phi(\Phi, a)|^2$ ALONG HOLLOW CYLINDER FOR E- POLARIZED INCIDENT RADIATION DIAMETER, D = LENGTH, L = 7" (17.8 cm)

This is close enough to $z = 0.192\lambda$ for us to normalize the Kao distribution to the measured distribution at $z = 0.192\lambda$ and $\phi = 40°$. What we observe is more or less general agreement of Kao theory with experimental results around this scan although the normalized theory seems to give a slightly lower current then was found by measurement. As we move along the tube to $z = 3L/8 = 0.288\lambda$ we observe in the empirical results the general increase in angular current amplitude that should appear as we approach the end of the tube. We find a minimum at $\phi = 0°$ a maximum five times as high at about $\phi = \pm 40°$ and then at $\phi \approx \pm 80°$ another minimum of about the same amplitude as that at $\phi = 0°$. Continuing on around the tube the squared amplitude of the angular component of the surface current increases to a second maximum at about $\phi = \pm 125°$. This maximum is only about half as high as the first one on the backside of the tube. Finally a minimum was measured at $\phi = 180°$. The amplitude at $\phi = 180°$ was measured and found to be about equal to that at the $\phi = \pm 80°$ minimum. We superimposed in figure 17 the Kao prediction for this current distribution after first normalizing it to the empirically observed value at $z = 0.288\lambda$ and $\phi = 40°$. The Kao results are actually for $z = 0.306\lambda$ and do not differ substantially from the theoretical values at $z = 0.288\lambda$ and were therefore normalized to the $z = 0.288\lambda$ scan. As we see in figure 17 Kao predicts pretty much the same maxima and minima although they occur at slightly different azimuthal positions than were found experimentally. The only essential difference is the somewhat lower amplitudes for

Kao's theoretical distributions to the experimental values at ϕ=180° results in significant quantitative disagreement on the shadow side

the normalized Kao predictions of the current amplitude, on the side facing the source, relative to the measured values. We also show in figure 17 the results obtained for the measured scan of $|K_\phi(\phi,a)|^2$ near the very end of the finite, open ended, thin walled conducting tube. We note that the distribution is very much like that at $z = 3L/8 = 0.288\lambda$ with substantial amplification of the amplitude except at $\phi = 0°$ and 180°. If we could measure closer to the edge we would probably find a further increase in amplitude. Unfortunately there is a concatenation of practical limitations that preclude ever getting to an edge of a real tube in the laboratory. For the angular current component we thus note that the Kao theory when appropriately normalized does give reasonably accurate predictions for the amplitude in the case of a short tube at E-polarized normal incidence.

The final case we considered is that of the same finite length tube normally irradiated by the same wavelength electromagnetic plane wave but this time with the incident electric field polarized normal to the cylinder axis. This is the H-polarized case. As we shall see in the course of the discussion that follows this particular diffraction problem is a very interesting one. Before proceeding to the experimental results themselves it is interesting and quite informative to pause and reflect on how the competing constraints inherent in this diffraction problem interact and produce the resulting current distributions.

To begin with the incident radiation, we recall, is directed broadside and normal to the diffracting target. The latter is a

tudes that are significant enough to include in figure 15. What

hollow circular cylindrical tube. The magnetic field of the incident electromagnetic plane wave is aligned parallel to the axis of the target cylinder i.e. we have H-polarization. The wavelength of the incident electromagnetic radiation exceeds the length of the cylinder it is irradiating and it fits 2.40 times around its circumference. The open-ended thin walled cylindrical tube has a sharp edge at each of its ends. Because of the geometry and corresponding symmetry we expect to have only an azimuthal component of surface current on the outside wall of the tube around the central circle, i.e. at $z = 0$. The angular distribution of this current component should, at the very least, qualitatively more or less closely resemble the current on an infinite circular cylinder with circumference to wavelength ratio $\gamma = 2.40$ for H-polarization. Since the target cylinder is smaller lengthwise than the wavelength of the exciting radiation K_ϕ or the azimuthal component of surface current is forced to vary slowly with z as we move away from the central circle towards the tube ends. As we approach very close to the ends of the cylindrical tube the azimuthal component must increase. The closer to the tube end we get the faster must this increase become. We thus observe the presence of two competing constraints. Near the tube center, $z \approx 0$, one effect will dominate. We should expect to find for $z = 0$ and for some region nearby, probably to less than halfway from the center to the tube end, there will be an angular component of surface current that is relatively independent of the longitudinal coordinate z. Out in the vicinity of the edges, or tube ends, the other requirement will dominate and the angular

in toward the center at $z=3\lambda/4$ we find the empirical results

component of current will increase around the tube over that at and near $z = 0$. This is most likely to become evident at $z > L/4$ i.e. closer to the ends than to the center. Over that portion of the tube in the vicinity of $z \approx L/4$ we should not be surprised to find some hybridization of effects due to both requirements. For some values of azimuth we may find K_ϕ increasing with z and for others it may be temporarily decreasing with respect to the longitudinal coordinate. Formal theoretical considerations require that K_ϕ becomes infinite at the actual tube ends. In any real laboratory situation, however, this is never realized since an end of a tube never fully achieves the required characteristics of the theoretical tube end. Practical limitations on physical dimensions of sensors preclude any measurement precisely at an ideal edge. Nevertheless, real sensors utilized for measuring on real tubes should reveal an increasing K_ϕ as z approaches L/2, the tube end. Since the diffracting cylinder is finite in length there is a longitudinal surface current component K_z on the outer wall of tube. This current component is identically zero around the tube for $z = 0$. This is due to the circular cylindrical geometry and mirror symmetry in the z-direction. Again the fact that the cylinder length is exceeded by the wavelength of the incident radiation requires that the axial or longitudinal component of surface current K_z be a relatively slowly varying function of z in the neighborhood of $z = 0$. This should persist out to about $z \lesssim L/4$. Now this surface current component is directed normal to the ends of the tube. Consequently as we approach the tube

testing the Kao analytic results. Since our second cylinder has a

ends this component, K_z, should fall off rapidly for all ϕ. We now have a component of surface current that is identically zero at $z = 0$ and again at $z = L/2$. This current must remain relatively small over the ranges $0 < z < L/4$ and $z \lesssim L/2$. Recall that the distance from the center of the tube to the end of the tube is $L/2 = 0.383\lambda$. This distance is appreciably less than half a wavelength. Thus we should expect to find for some small range of z, imbedded in $L/2 > z > L/4$, that the longitudinal component of current on the outer wall of the cylindrical tube experiences a significant increase over that near the center and ends of the tube. Nevertheless, this component for a real tube should stay quite small over the entire tube. Thus as z increases from the center we should expect K_z to be identically zero at zero, increase slowly at first then more rapidly out beyond $z = L/4$ and, thereafter attenuate very rapidly as z approaches the tube end at L/2. Upon reflection then we can conclude that for this case of a "short," fat, uncapped, circular, conducting tube at H-polarization except perhaps at the very end of the finite tube we have the closest approximation to infinite cylinder behaviour, this is true at least for the exterior surface currents. We next consider the results obtained in the laboratory for the distribution of the induced surface currents over this cylinder which we state in advance and shall shortly see do indeed corroborate this prediction of the response of the tube.

Figure 18 displays the results of measurement of the angular distribution of the squared amplitude of the azimuthal component of surface current at several longitudinal positions along the finite

were made around circles in planes through the center of the cylinder,

length circular cylindrical tube. It also contains the corresponding theoretical prediction for the current on the outside wall of an infinitely long circular cylinder for H-polarization. What the infinite cylinder theory predicts for $|K_\phi(\phi,a)|^2$ is a maximum at $\phi = 0°$ followed by a minimum at about $\phi = \pm 27°$. As the azimuthal coordinate advances around the cylinder the infinite cylinder current amplitude squared rises steadily, passes through an inflection point at about $\phi = \pm 80°$ and then continues to increase as ϕ increases until it attains a high peak at a maximum at $\phi = 180°$. Since all the experimental curves for $|K_\phi|^2$ passed through a common point for $\phi = \pm 30°$ we normalized the infinite cylinder results to the value of $|K_\phi|^2/|H_o|^2$ at $z = 0$ and $\phi = \pm 30°$. This normalized infinite cylinder current distribution is the one shown in figure 18. The height at the high peak at $\phi = 180°$ is about five times that at the peak at $\phi = 0°$ and about 2.5 times that at the inflexion point near $\phi = \pm 80°$. Also the infinite cylinder predicts that the peak value of $|K_\phi|^2$ at $\phi = 0°$ is about four times the value of $|K_\phi|^2$ at the minimum near $\phi = \pm 27°$. At $z = 0$ the measured values of the distribution of $|K_\phi|^2$ should most closely be approximated by the infinite cylinder predictions. What we find empirically is a maximum at $\phi = 0°$ followed by a minimum at about $\phi = \pm 27°$. Instead of an inflection point near the top and bottom of the finite cylinder we find empirically the current distribution has been resolved so as to show a maximum at about $\phi = \pm 70°$ and then a slight drop to a minimum at about $\phi = \pm 85°$. This is then followed by a monotonic increase to a maximum at $\phi = 180°$. The ratio of $|K_\phi|^2$ at the two

Let us next proceed to examine the experimentally obtained surface current distribution on the short, open tube for E-polarization of

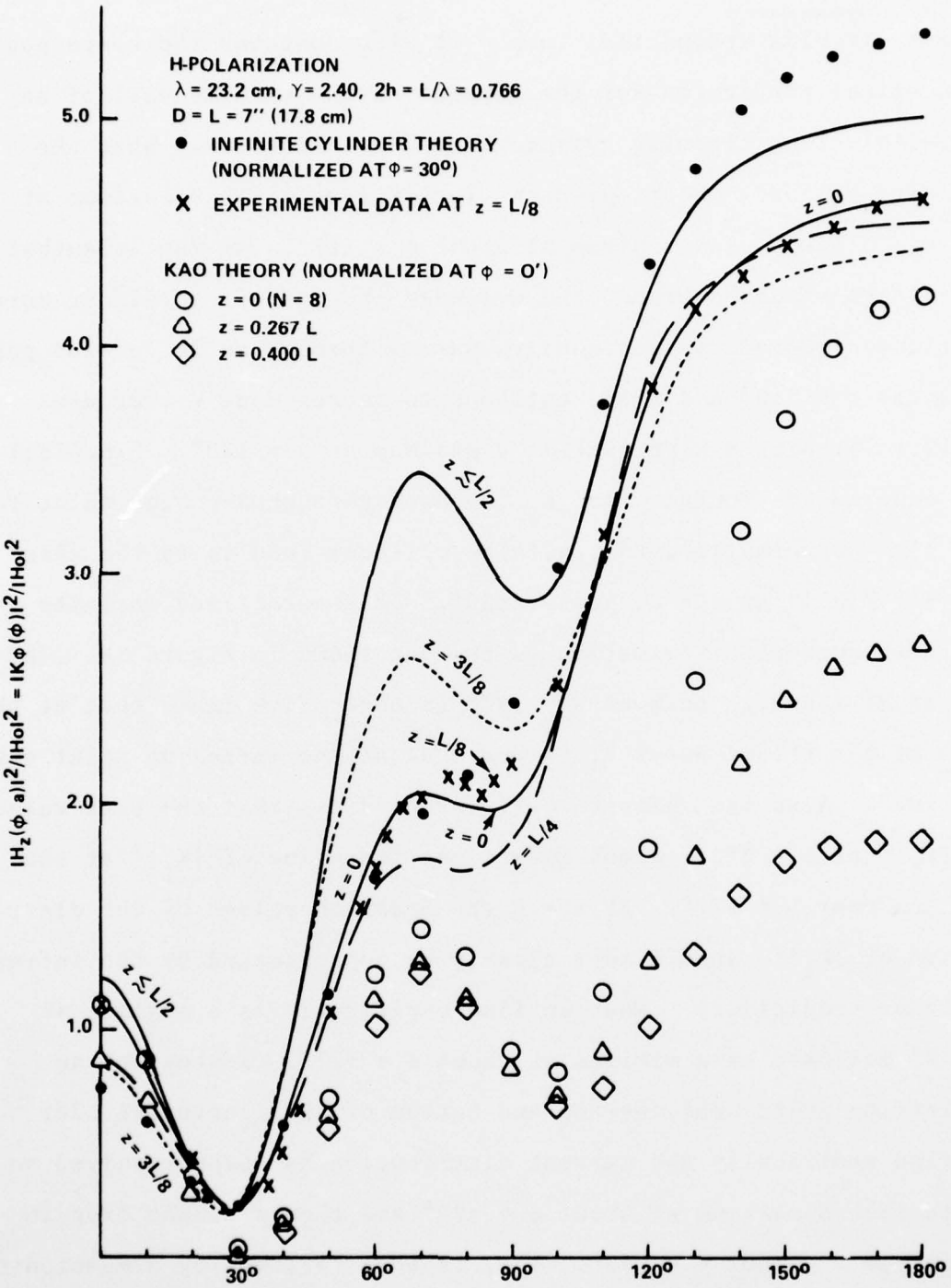

FIG. 18 ANGULAR DISTRIBUTION OF SURFACE CURRENT $|K_\phi|^2$ ALONG HOLLOW CYLINDER OF DIAMETER D = 7" (17.8 cm) = LENGTH L.

measured current $|K_z|^2$ at the maximum at $\phi = 180°$ is only about four

peaks $\phi = 180°$ and $\phi = 0°$ is about five to one. At $\phi = 180°$ the peak height of $|K_\phi|^2$ is just a bit less than 2.5 times the average peak height of $|K_\phi|^2$ over the range $\phi = \pm 70°$ to $\phi = \pm 90°$. Also the measured peak height at $\phi = 0°$ is about four times the measured value of $|K_\phi|^2$ at the minimum near $\phi = \pm 27°$. Thus except for the detailed structure in the distribution from $\phi \approx 70°$ to $\phi \approx 90°$ the measured angular distribution of $|K_\phi(\phi,a)|$ at $z = 0$ for the finite tube is qualitatively very similar to the normalized predictions of infinite cylinder theory. Even in the range of $\phi \approx 70°$ to $\phi \approx 90°$ there is no really outstanding difference from the normalized infinite cylinder distributions. Quantitatively we find the measured distribution for $|K_\phi|$ at $z = 0$ at worst only lies slightly above the normalized infinite cylinder predictions for angular position ϕ less than about 75°. Thereafter it lies below the normalized infinite cylinder predictions. Actually for most of the range it differs from the normalized infinite cylinder theory predictions by about 13%. Note next that if we move out along the finite tube to $z = L/8 = 0.096\lambda$ the measured angular scan of $|K_\phi(\phi)|^2$ nearly coincides with that for $z = 0$. The principal difference can be seen near the top and bottom of the finite length tube where just around on the shadow side the structural detail consisting of a minimum and a maximum is sharpened up a bit for $z = L/8$ over that for $z = 0$. Moving further out towards the ends of the tube to $z = L/4 = 0.192\lambda$ we find precisely the same qualitative characteristics for $|K_\phi(\phi,a)|^2$. The positions of the minima can be seen in figure 18 to have shifted slightly towards $\phi = 0°$. For $|\phi|$ less

than about 107° the measured $|K_\phi|^2$ at worst lies below the measured $|K_\phi|^2$ for z = 0. It then lies slightly higher than the z = 0 current distribution up to about $\phi = \pm 148°$. Thereafter it lies below that distribution. For z = L/4 the maximum and minimum just before $\phi = \pm 90°$ occur over a smaller range of azimuth and hence appear somewhat more strongly emphasized. At $z = 3L/8 = 0.288\lambda$ we are closer to the tube end than to the tube center. The measurements show that up to about $\phi = \pm 30°$ $|K_\phi|^2$ is pretty nearly the same for z = 3L/8 as for z = L/4. Then as ϕ increases the distribution at z = 3L/8 rises above and remains above the z = 0 and z = L/4 distributions up to about $\phi = \pm 107°$. At that point we are around on the front side of the tube facing the incoming radiation. As ϕ then increases on around to 180° the z = 3L/8 distribution for $|K_\phi(\phi,a)|$ lies below that for z = 0 and that for z = L/4. Over this latter range of azimuthal position all three distributions lie pretty close together. We do see a spread of the fine structure at the top and bottom of the tube for z = 3L/8. The maximum is at about $\phi = \pm 67°$ and the minimum at about $\phi = \pm 88°$. In addition to the spread in ϕ there is now a sharper increase in the ratio of height at maximum to that at minimum. As we expect the greatest changes occur as the tube end is approached. We measured the angular distribution of $|K_\phi(\phi,a)|^2/|H_o|^2$ quite close to the end at $z \lesssim L/2$. Because of practical limitations it is impossible to get accurate measurements at z = L/2. We observe from the results that out near the ends $|K_\phi|$ assumes its largest values for the range of azimuth from $\phi = 0°$ to about $\phi = \pm 20°$. A maximum occurs at $\phi = 0°$ of course.

amplitude of this component of surface current all around the tube.

A minimum was observed at this outermost scan that lies at about $\phi = \pm 27°$. In the vicinity of this minimum $|K_\phi|$ drops slightly below the values obtained for scans taken closer to the tube center. As the angle ϕ increases the $z \lesssim L/2$ scan of $|K_\phi|^2$ nearly coincides with that for $z = 3L/8$ and both lie above all the other scans. This characteristic persists until about $\phi = \pm 45°$. From that azimuthal position on around to $\phi = 180°$ on the incident side the angular distribution of $|K_\phi(\phi,a)|$ for the outermost longitudinal position rises rather significantly above all the other angular scans of $|K_\phi(\phi,a)|$. The region in which the minimum and maximum occur near the top and bottom of the finite tube is enlarged and now ranges from about $\phi = \pm 45°$ to about $\phi = \pm 110°$. At this outermost scan the maximum is at about $\phi = \pm 70°$ and is pretty much at the same azimuthal position as found for the inner scans. The minimum on the other hand has moved further around to the incident side to about $\phi = \pm 95°$. At $\phi = 0°$ the peak height for $|K_\phi|^2$ is only slightly higher and about equal to that for $z = 0$. At the intermediate peak near $\phi = \pm 70°$ the measured $|K_\phi|^2$ for $z \lesssim L/2$ is about 1.5 times that for $z = 0$. At $\phi = 180°$ $|K_\phi|^2$ for the outer scan is only about 7-8% higher than the value obtained for $|K_\phi|^2$ at $z = 0$. All in all we note in summary that the measured results for $|K_\phi|^2$ over the finite tube are in good agreement with what we should have expected for this physical quantity.

We also show in figure 18 the angular distributions for $|K_\phi(\phi,a)|^2$ predicted by C. C. Kao. Since all of these theoretical distributions have extremely small amplitudes at $\phi = \pm 30°$ we normalized the angular distributions for each value of z to the measured results at $\phi = 0°$.

this new maximum is about equal in amplitude to that at $\phi = 0°$ and is

This then facilitates comparing the results from the approximate theory of Kao to both the measured data and infinite cylinder theory. The Kao theory of course is formulated to cause $|K_\phi|$ to become singular at $z = L/2$. For each angular distribution we find a maximum at $\phi = 0°$ and another at $\phi = 180°$. Similar to the measured results we observe not an inflexion point near the top and bottom of the tube but a maximum and minimum. Also Kao predicts a minimum near $\phi = \pm 30°$ in agreement with infinite cylinder theory and the measured results. Even though we find these qualitative characteristics in relatively good agreement the same does not appear true for the quantitative behavior of Kao's results. The most striking deviation probably occurs near $\phi = \pm 30°$ where the Kao theory predicts the occurrence of pretty nearly a null in $|K_\phi|$ for all $z < L/2$. This does not occur in the infinite cylinder prediction nor in the measured results for $z = 0$ (or for any measured scan at the other z positions). The intermediate maxima for each z is predicted to lie at about $\phi = \pm 70°$ in agreement with the measurements. The accompanying minimum according to the Kao theory lies on the incident side of the finite length tube. For each value of z the Kao position of this minimum is at $\phi = \pm 100°$. Only the corresponding minimum for the outermost experimental scan of $|K_\phi|^2$ approximates to this characteristic. Overall we note that the normalized Kao angular distribution for $|K_\phi|^2$ for $z = 0$ is not greatly different from the measured results for $\phi < \pm 25°$, $35° < \phi < 80°$ and for $\phi > 155°$. There is a much larger discrepancy that is quite evident for the remaining

length tube similarly irradiated does have an angular component of

azimuthal values. For larger z or greater distances from the center we observe in figure 18 that the normalized Kao theory predicts for $\phi>90°$ that $|K_\phi|^2$ decreases as z increases. This is finally offset by the theory giving infinite $|K_\phi|^2$ at $z = L/2$. All in all the normalized Kao theory predicts angular distributions of $|K_\phi(\phi,a)|^2$ that are too low in value for $\phi>25°$ for all values of longitudinal coordinates $z < L/2$. For $z = 0$ the normalized Kao theory gives an angular distribution that is too far out of agreement with the infinite cylinder prediction for $|K_\phi(\phi,a)|^2$.

Let us now turn our attention to the other component of surface current on the outer wall of the finite length tube. We repeat that this component does not exist for the infinite circular cylinder at H-polarization. In figure 19 we display the measured results for $|K_z(\phi,a)|^2/|H_o|^2$ at various positions z along the length of the tube. For $z = 0$ we found $|K_z|^2$ is identically zero for all ϕ. At $z = L/8$ the signal for $|K_z|^2$ is well imbedded in the noise. Thus for all ϕ this measured angular distribution is quite close to zero also. For $z = 0$ Kao's theory "a priori" gives $|K_z|^2 \equiv 0$ for all ϕ. For $z = 0.102\lambda \approx L/8$ Kao's theory still predicts a very small, almost zero amplitude for K_z for all ϕ. Thus at least near the center line of the finite length circular cylindrical tube the measurements are coincident with infinite cylinder theory and the approximate Kao theory. At $z = L/4 = 0.192\lambda$ the measured results indicate a null for $|K_z(\phi,a)|^2$ at $\phi = 0°$. As ϕ increases $|K_z|^2$ increases for $z = L/4$ and attains a small maximum at about $\phi = \pm 37°$.

shown in figure 17 is the Kao prediction for $|K_\phi(\phi,a)|^2$ at $z = 0.204\lambda$.

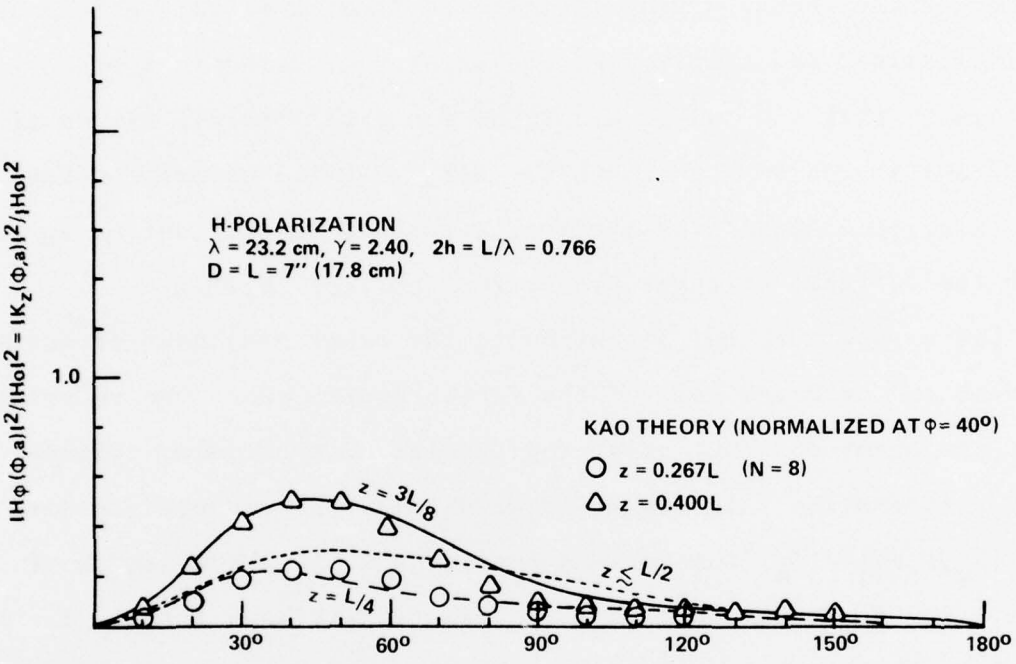

FIG. 19 ANGULAR DISTRIBUTION OF SURFACE CURRENT $|K_z|^2$ ALONG HOLLOW CYLINDER OF DIAMETER D=7" = LENGTH L.

Thereafter as ϕ increases $|K_z(\phi,a)|$ decreases relatively rapidly at first and then very slowly from about $\phi = \pm 60°$ to another null at $\phi = 180°$. As we show in figure 19 the Kao theoretical values for $z = 0.267L \approx L/4$ normalized to $\phi = 40°$ and $z = L/4$ give pretty much the same results for $|K_z(\phi,a)|$ as the measurements. The maximum for the Kao result occurs for a larger value of azimuth, somewhere about $\phi = \pm 43°$. As we move further away from the center line of the cylinder and are closer to the tube end we find for example the measured angular distribution shown in figure 19 for $z = 3L/8$. There is again a null at $\phi = 0°$ and then a maximum at about $\phi = \pm 43°$. As ϕ increases further the measured $|K_z|^2$ falls off just as fast as it climbed up to the maximum. From $\phi \approx 80°$ on it then attenuates at a much slower rate and vanishes at $\phi = 180°$. The Kao results for a z slightly further out, $z = 0.400L$, were normalized to the measured results at $z = 3L/8$ and $\phi = 40°$. As can be seen in figure 19, the normalized Kao distribution for $|K_z(\phi,a)|^2$ nearly coincides with the measured results except near the top and bottom of the tube where it falls somewhat lower than was observed empirically. Thus far we find that $|K_z(\phi,a)|$ is behaving both experimentally and theoretically as we expected it to. Kao's theory has two adjustable parameters that force $|K_z(\phi,a)|$ to vanish at $z = \pm L/2$ i.e. at the ends of the finite length tube. As we approach the tube end in the laboratory we find that $|K_z(\phi,a)|$ does indeed attenuate considerably. In figure 19 we show for $z \lesssim L/2$ the measured $|K_z(\phi,a)|^2$ distribution. It has a null at

The only essential difference is the somewhat lower amplitudes for

$\phi = 0°$ and also at $\phi = 180°$. In addition it indicates a maximum around $\phi = \pm 50°$. Overall it shows a slow variation in height for all ϕ and a general decrease from the angular distribution measured for $z = 3L/8$.

In summary then both $|K_z(\phi,a)|$ and $|K_\phi(\phi,a)|$ exhibit empirically just the behaviour we can expect to find for this diffraction problem. The Kao theory is somewhat better able to handle this short cylinder at H-polarization. If one considers that the average $|K_z(\phi,a)|$ for each fized z-scan is rather small we find that unless great detail is needed the normalized infinite cylinder theory pretty well describes the finite cylinder surface current distribution and will prove adequate for most practical situations to approximate to the short cylinder at H-polarization. The behaviour at the very end of the tube will still require some additional improvement over the infinite cylinder theory.

AD-A041 199 STATE UNIV OF NEW YORK AT ALBANY F/G 20/14
SCATTERING OF ELECTROMAGNETIC RADIATION BY APERTURES: XI. THE O--ETC(U)
MAR 77 J P HECKL, L F LIBELO, C L ANDREWS N60921-75-C-0131
UNCLASSIFIED NSWC/WOL-TR-76-74 NL

2 OF 2
AD
A041199

END

DATE
FILMED
7-77

IV. CONCLUSIONS AND SUMMARY

We have presented the results of resonance region measurements of internal fields at the axis of a finite cylinder of circular cross-section illuminated normally by E-polarized plane electromagnetic radiation. One of the more interesting consequences of these measurements was the observation that an incident longitudinally polarized wave can drive the open tube ends and thereby launch in the interior a radial distribution of electric field. Although in the particular problem investigated and reported on here this was found to be an inefficient mechanism to produce this cross polarization excitation it does not necessarily follow that this is an insignificant phenomenon in general. Results of a second investigation namely the measurement of the surface charge density distribution on the inner curved wall of the open ended circular tube of finite length induced by H-polarized incident radiation were also presented and discussed. These are probably the first measurements of the internal surface charge density distribution for a short fat open cylindrical tube of length about $3\lambda/4$ and for a similar but longer tube of length about $5\lambda/2$. We also presented and discussed the measured surface charge density distribution on the outer wall of these open cylindrical tubes. Again these are probably the first such measurements reported on for such finite length tubes. Finally we discussed the empirical results obtained for the current density distribution on the outside wall of each of these tubes for both E-polarized and H-polarized incident electromagnetic plane waves.

We compared where appropriate the predictions of infinite cylinder theory for amplitudes of charge densities and components of surface current to the corresponding measured quantities and assessed the reliability of approximating via the simple infinite cylinder theory. In addition we compared, wherever we could, the predicted distributions using the theory developed by Kao. Generally we found that this latter approximate analytic approach did not yield sufficiently reliable results. Although for shorter length cylinders it gave relatively better predictions.

We have investigated an extreme case of apertures in a conducting body of finite dimensions subjected to irradiation by a plane wave of wavelength comparable in size to these characteristic dimensions. The symmetry observed empirically in $|K_j(\phi)|^2$ and $|\sigma(\phi)|^2$ relative to the ϕ and z coordinates requires that the field components on and inside the open ended tubes must satisfy some very important symmetry requirements themselves. By utilizing these experimentally obtained results major simplifications can be made in the coupled simultaneous equations that appear when a purely analytic solution is attempted for the finite cylinder diffraction problem. We shall show in subsequent reports how this does indeed facilitate the theoretical solution of this rather difficult problem.

REFERENCES

1. R. L. Kligman, L. F. Libelo, "S.E.R.A. VIII. The Normally Slotted Infinite Cylinder-Theory" NOLTR 74-35 June 1974.

2. L. F. Libelo, C. L. Andrews, "S.E.R.A. IX. Surface Current Distributions Over a Closed Cylindrical Can at Broadside Incidence," NSWC/WOL/TR 75-163 February 1976.

3. J. Van Bladel, "Electromagnetic Fields" p. 376-382, McGraw-Hill Book Co., New York, N. Y. 1964.

4. J. J. Bowman, T.B.A. Senior and P.L.E. Uslenghi, eds. "Electromagnetic and Acoustic Scattering by Simple Shapes" pp. 92-93, North Holland Co., Amsterdam, the Netherlands 1969.

5. R.W.P. King and T.T. Wu, "Scattering and Diffraction of Waves," p. 38, Harvard Univ. Press, Cambridge, Mass. 1959.

6. W. Panofsky and M. Phillips, "Classical Electricity and Magnetism" p. 199-301 Addison-Wesley Publishing Co., Reading, Mass. 1956.

7. J. R. Wait, "Electromagnetic Radiation from Cylindrical Structures," p. 142, Pergamon Press, New York 1959.

8. L. F. Libelo, C. L. Andrews, "S.E.R.A. IX. Surface Current Distribution over a Closed Cylindrical Can at Broadside Incidence," NSWC/WOL/TR 75-163, February 1976.

9. T. T. Wu, "Introduction to Linear Antennas," Chapt. 8 of "Antenna Theory," Part I by R. E. Collin and F. J. Zucker, McGraw-Hill Book Company, New York, 1969.

10. D. C. Chang, "On the Electrically Thick Monopole Part I - Theoretical Solution," IEEE Trans. Ant. and Prop. AP-16, 58 (1968).

11. D. C. Chang, "On the Electrically Thick Cylindrical Antenna," Tech. Rept. 509 Cruft Laboratory, Harvard Univ., Cambridge, Mass. 1966.

12. S. R. Seshadri, T. T. Wu, "An Integral Equation for the Current In an Asymmetrically Driven Antenna," Proc. IEEE 55, 1097 (1967).

13. T. T. Wu, R.W.P. King, "The Thick Tubular Transmitting Antenna," Radio Sci., 2, 1088 (1967).

REFERENCES (CONT.)

14. C. C. Kao, "Three Dimensional Electromagnetic Scattering From a Circular Tube of Finite Length," Jour. Appl. Phys. 40, 4732 (1969).

15. C. C. Kao, "Electromagnetic Scattering From a Finite Tubular Cylinder: Numerical Solutions and Data I. Development of Theory," AFCRL-69-0535(I) Cruft Laboratory, Harvard Univ., Cambridge, Mass. 1969.

16. C. C. Kao, "Electromagnetic Scattering From a Finite Tubular Cylinder: Numerical Solutions and Data II. Numerical Results," AFCRL-69-0535(II) Cruft Laboratory, Harvard Univ., Cambridge, Mass. 1969.

17. C. C. Kao, "Electromagnetic Scattering From a Finite Tubular Cylinder: Numerical Solutions," Radio Sci. 5, 617 (1970).

18. A. Young, "Approximate Product Integration," Proc. Roy. Soc. A-224, 552 (1954).

19. A. Young, "The Application of Approximate Product-Integration to the Numerical Solution of Integral Equations," Proc. Roy. Soc. A-224, 561 (1954).

20. C. C. Kao, "Measurements of Surface Currents On a Finite Circular Tube Illuminated by an Electromagnetic Wave," IEEE Trans. on Ant. and Prop. AP-18, 569 (1970).

21. R. O. Dell, C. R. Carpenter and C. L. Andrews, "Optical Design of Anechoic Chambers," Jour. Opt. Soc. Amer., 902, 62 (1972).

22. C. L. Andrews, A. Golab, "Probe Antennas for Microwave Measurements," Amer. Jour. Phys. 121, 39 (1971).

DISTRIBUTION

Copies

Director
Defense Advanced Research Project Agency
Architect Building
1400 Wilson Blvd
Arlington, Virginia 22209
ATTN: Technical Library

Defense Communication Engineer Center
1860 Wiehle Avenue
Reston, Virginia 22090
ATTN: Code R124C Technical Library

Director
Defense Communications Agency
Washington, D.C. 20305
ATTN: Technical Library

Defense Documentation Center
Cameron Station
Alexandria, Virginia 22314
ATTN: TC 12

Director
Defense Intelligence Agency
Washington, D.C. 20301
ATTN: Technical Library

Director
Defense Nuclear Agency
Washington, D.C. 20305
ATTN: RAEV
ATTN: RATN
ATTN: STVL
ATTN: STTL Technical Library 2
ATTN: STSI Archives

Director
National Security Agency
Ft. George G. Meade, Maryland 20755
ATTN: Technical Library

DISTRIBUTION (CONT.)

Copies

Director
BMD Advanced Technical Center
Huntsville Office
P.O. Box 1500
Huntsville, Alabama 35807
ATTN: Technical Library

Chief of Res, Dev & Acquisition
Department of the Army
Washington, DC 20310
ATTN: DAMA-CSM-N LTC E. V. Deboeser, Jr.

Commander
Harry Diamond Laboratories
2800 Powder Mill Road
Adelphi, Maryland 20783
ATTN: AMXDO-TI Technical Library
ATTN: AMXDO-RB Joseph R. Miletta

ATTN: AMXDO-EM J. M. Bombardt

Commander
Picatinny Arsenal
Dover, New Jersey 07801
ATTN: Technical Library

Commander
Redstone Scientific Information Center
U.S. Army Missile Command
Redstone Arsenal, Alabama 35809
ATTN: AMSMI-RBD Clara T. Rogers

Director
U.S. Army Ballistic Research Laboratories
Aberdeen Proving Ground, Maryland 21005
ATTN: Technical Library Edward Baicy

Commander
U.S. Army Communications Command
Fort Huachuca, Arizona 85613
ATTN: Technical Library

Chief
U.S. Army Communications System Agency
Fort Monmouth, New Jersey 07703
ATTN: SCCM-AD-SV Library

DISTRIBUTION (CONT.)

Copies

Commander
White Sands Missile Range
White Sands Missile Range, New Mexico 88002
ATTN: Technical Library

Chief of Naval Research
Navy Department
Arlington, Virginia 22217
ATTN: Technical Library
ATTN: Code 464 Thomas P. Quinn

Commander
Naval Air Systems Command
Headquarters
Washington, DC 21360
ATTN: Technical Library

Commander
Naval Electronic Systems Command
Naval Electronic Systems Command Headquarters
Washington, DC 20360
ATTN: Technical Library

Commander
Naval Ocean Systems Center
San Diego, California 92152
ATTN: Technical Library
ATTN: Code 2200 1 Verne E. Hildebrand

Commanding Officer
Naval Intelligence Support Center
4301 Suitland Road, Bldg. 5
Washington, DC 20390
ATTN: Technical Library

Superintendent
Naval Postgraduate School
Monterey, California 93940
ATTN: Code 2124 Technical Reports Librarian

Director
Naval Research Laboratory
Washington, DC 20375
ATTN: Code 2027 Technical Library

DISTRIBUTION (Cont.)

Copies

Headquarters
Air Force Systems Command
Andrews AFB
Washington, D.C. 20331
ATTN: Technical Library

Commander
Air University
Maxwell AFB, Alabama 36112
ATTN: AUL/LSE-70-250

Headquarters
Electronic Systems Division, (AFSC)
L. G. Hanscom Field
Bedford, Massachusetts 01730
ATTN: Technical Library

Commander
Foreign Technology Division, AFSC
Wright-Patterson AFB, Ohio 45433
ATTN: TD-BTA Library

Headquarters USAF/RD
Washington, D.C. 20330
ATTN: RDQPN

Commander
Rome Air Development Center, AFSC
Griffiss AFB, New York 13440
ATTN: EMTLD DOC Library

Division of Military Application
U.S. Energy Research and Development Administration
Washington, D.C. 20545
ATTN: DOC CON for Class Technical Library

EG&G, Inc.
Los Alamos Division
P.O. Box 809
Los Alamos, New Mexico 85544
ATTN: Technical Library

AF Weapons Laboratory, AFSC
Kirtland AFB, New Mexico 87117
ATTN: EL (Library)

DISTRIBUTION (Cont.)

Copies

University of California
Lawrence Livermore Laboratory
P.O. Box 808
Livermore, California 94550
ATTN: Technical Info Dept L-3
ATTN: J. N. Brittingham

Los Alamos Scientific Laboratory
P.O. Box 1663
Los Alamos, New Mexico 87545
ATTN: Doc Control for Reports Library

Sandia Laboratories
P.O. Box 5800
Albuquerque, New Mexico 87115
ATTN: Doc Control for Sandia Rpt Coll
ATTN: Doc Control for DRG 9353 R. L. Parker

U.S. Energy Research and Development Administration
Albuquerque Operations Office
P.O. Box 5400
Albuquerque, New Mexico 87115
ATTN: Doc Control for Technical Library

Battelle Memorial Institute
505 King Avenue
Columbus, Ohio 43201
ATTN: Technical Library

Department of Commerce
National Bureau of Standards
Washington, D.C. 20234
ATTN: Technical Library

Department of Commerce
National Oceanic and Atmospheric Administration
Environmental Research Laboratories
Boulder, Colorado 80302
ATTN: Classified Document Library

NASA
600 Independence Avenue S.W.
Washington, D.C. 20546
ATTN: Code Res Guid Con & Info Sys
ATTN: Technical Library

DISTRIBUTION (Cont.)

Copies

Franklin Institute, The
20th Street and Parkway
Philadelphia, Pennsylvania 19103
ATTN: Technical Library

Computer Sciences Corporation
P.O. Box 530
6565 Arlington Blvd
Falls Church, Virginia 22046
ATTN: Technical Library

Computer Sciences Corporation
201 La Veta Drive N.E.
Albuquerque, New Mexico 87108
ATTN: Alvin T. Schiff

Cutler-Hammer, Inc.
AIL Division
Comac Road
Deer Park, New York 11729
ATTN: Central Tech Files Anne Anthony

Denver, University of
Colorado Seminary
P.O. Box 10127
Denver, Colorado 80210
ATTN: Sec Officer for Technical Library

Dikewood Corporation, The
1009 Bradbury Drive, S.E.
University Research Park
Albuquerque, New Mexico 87106
ATTN: Technical Library

E-SYSTEMS, Inc.
Greenville Division
P.O. Box 1056
Greenville, Texas 75401
ATTN: Library 8-50100

General Electric Company
Space Division
Valley Forge Space Center
Goddard Blvd King of Prussia
P.O. Box 8555
Philadelphia, Pennsylvania 19101
ATTN: Technical Information Center

DISTRIBUTION (Cont.)

Copies

Johns Hopkins University
Applied Physics Laboratory
Johns Hopkins Road
Laurel, Maryland 20810
ATTN: Technical Library

Kaman Sciences Corporation
P.O. Box 7463
Colorado Springs, Colorado 80933
ATTN: W. Foster Rich
ATTN: Walter E. Ware
ATTN: Library

National Academy of Sciences
ATTN: National Materials Advisory Board
2101 Constitution Avenue
Washington, D.C. 20418
ATTN: R. S. Shane Nat Materials Advsy

IIT Research Institute
Electronmag Compatability Anal Center
North Severn
Annapolis, Maryland 21402
ATTN: Technical Library

IIT Research Institute
10 West 35th Street
Chicago, Illinois 60616
ATTN: Technical Library
ATTN: Irving N. Mindel

Institute for Defense Analyses
400 Army-Navy Drive
Arlington, Virginia 22202
ATTN: IDA Librarian Ruth S. Smith

M.I.T. Lincoln Laboratory
P.O. Box 73
Lexington, Massachusetts 02173
ATTN: Librarian A-082

McDonnell Douglas Corporation
P.O. Box 516
St. Louis, Missouri 63166
ATTN: Technical Library
ATTN: A. C. Lind

DISTRIBUTION (Cont.)

Copies

Stanford Research Institute
333 Ravenswood Avenue
Menlo Park, California 94025
ATTN: SRI Library, Room G021

Palisades Inst for Research Services, Inc.
201 Varick Street
New York, New York 10014
ATTN: Records Supervisor

Perkin-Elmer Corporation
Main Avenue
Norwalk, Connecticut 06852
ATTN: Technical Library

Sidney Frankel & Associates
1165 Saxon Way
Menlo Park, California 94025
ATTN: Sidney Frankel

R&D Associates
P.O. Box 9695
Marina Del Rey, California 90291
ATTN: Technical Library

Rand Corporation, The
1700 Main Street
Santa Monica, California 90406
ATTN: Technical Library

Raytheon Company
Hartwell Road
Bedford, Massachusetts 01730
ATTN: Library
ATTN: Gajanan H Joshi Radar Sys Lab

Sperry Microwave Electronics Div
Sperry Rand Corporation
P.O. Box 4648
Clearwater, Florida 33518
ATTN: Technical Library

Department of Physics
State University of New York at Albany
Albany, New York 12203
Dr. C. L. Andrews

DISTRIBUTION (Cont.)

Copies

Electrical Engineering Dept.
University of Arizona
Tucson, Arizona 85721
Dr. D. Dudley

Physics Department
Youngstown University
Youngstown, Ohio 44503
Dr. P. Dalbec

Electrical Engineering Dept.
University of West Virginia
Morgantown, West Virginia 26506
Dr. C. Balanis

McDonnell-Douglas Corp.
St. Louis, Missouri 63166
Dr. A. C. Lind

Chemistry Department
University of Puerto Rico
San Juan, Puerto Rico
Dr. L. Veguilla-Berdecia